Cell

A Phase Ib Trial of Personalized Neoantigen Therapy Plus Anti-PD-1 in Patients with Advanced Melanoma, Non-small Cell Lung Cancer, or Bladder Cancer

Graphical Abstract

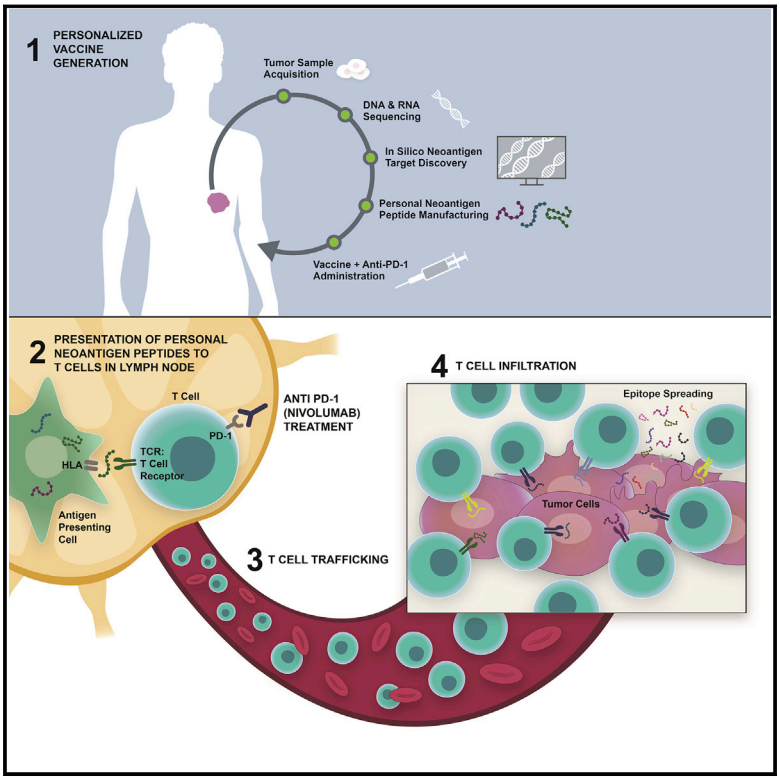

Authors

Patrick A. Ott, Siwen Hu-Lieskovan, Bartosz Chmielowski, ..., Mark DeMario, Richard B. Gaynor, Lakshmi Srinivasan

Correspondence

patrick_ott@dfci.harvard.edu (P.A.O.), lakshmi.srinivasan@biontech.us (L.S.)

In Brief

In a phase Ib clinical trial, Ott et al. demonstrate feasibility, safety, and immunogenicity of the combination of personalized neoantigen vaccines and PD-1 inhibition in patients with advanced solid tumors. Vaccine-induced T cells persist over time, exhibit cytotoxic potential, and can migrate to tumors. Epitope spread and major pathologic tumor responses were detected following vaccination.

Highlights

- The personalized neoantigen vaccine Neo-PV-01 plus nivolumab is feasible and safe
- NEO-PV-01 plus nivolumab stimulates durable neoantigen-specific T cell reactivity
- NEO-PV-01-specific T cells have cytotoxic potential and can traffic to the tumor
- NEO-PV-01 induces epitope spreading consistent with vaccine-mediated tumor cytotoxicity

Ott et al., 2020, Cell *183*, 347–362
October 15, 2020
https://doi.org/10.1016/j.cell.2020.08.053

CellPress

Cell

CellPress

Article

A Phase Ib Trial of Personalized Neoantigen Therapy Plus Anti-PD-1 in Patients with Advanced Melanoma, Non-small Cell Lung Cancer, or Bladder Cancer

Patrick A. Ott,[1,*] Siwen Hu-Lieskovan,[2] Bartosz Chmielowski,[2] Ramaswamy Govindan,[3] Aung Naing,[4] Nina Bhardwaj,[5] Kim Margolin,[6] Mark M. Awad,[1] Matthew D. Hellmann,[7] Jessica J. Lin,[8] Terence Friedlander,[9] Meghan E. Bushway,[10] Kristen N. Balogh,[10] Tracey E. Sciuto,[10] Victoria Kohler,[10] Samantha J. Turnbull,[10] Rana Besada,[10] Riley R. Curran,[10] Benjamin Trapp,[10] Julian Scherer,[10] Asaf Poran,[10] Dewi Harjanto,[10] Dominik Barthelme,[10] Ying Sonia Ting,[10] Jesse Z. Dong,[10] Yvonne Ware,[10] Yuting Huang,[10] Zhengping Huang,[10] Amy Wanamaker,[10] Lisa D. Cleary,[10] Melissa A. Moles,[10] Kelledy Manson,[10] Joel Greshock,[10] Zakaria S. Khondker,[10] Ed Fritsch,[10] Michael S. Rooney,[10] Mark DeMario,[10] Richard B. Gaynor,[10] and Lakshmi Srinivasan[10,11,*]

[1]Dana Farber Cancer Institute, Brigham and Women's Hospital, and Harvard Medical School, Boston, MA, USA
[2]Department of Medicine, University of California, Los Angeles, Los Angeles, CA, USA
[3]Washington University School of Medicine, St. Louis, MO, USA
[4]Department of Investigational Cancer Therapeutics, The University of Texas MD Anderson Cancer Center, Houston, TX, USA
[5]Tisch Cancer Institute, Icahn School of Medicine, New York, NY, USA
[6]Department of Medical Oncology and Therapeutics Research, City of Hope National Medical Center, Duarte, CA, USA
[7]Memorial Sloan Kettering Cancer Center, New York, NY, USA
[8]Cancer Center, Massachusetts General Hospital, and Harvard Medical School, Boston, MA, USA
[9]Department of Medicine, Division of Hematology and Oncology, University of California, San Francisco, San Francisco, CA, USA
[10]Neon Therapeutics/BioNTech US, Cambridge, MA, USA
[11]Lead Contact
*Correspondence: patrick_ott@dfci.harvard.edu (P.A.O.), lakshmi.srinivasan@biontech.us (L.S.)
https://doi.org/10.1016/j.cell.2020.08.053

SUMMARY

Neoantigens arise from mutations in cancer cells and are important targets of T cell-mediated anti-tumor immunity. Here, we report the first open-label, phase Ib clinical trial of a personalized neoantigen-based vaccine, NEO-PV-01, in combination with PD-1 blockade in patients with advanced melanoma, non-small cell lung cancer, or bladder cancer. This analysis of 82 patients demonstrated that the regimen was safe, with no treatment-related serious adverse events observed. *De novo* neoantigen-specific $CD4^+$ and $CD8^+$ T cell responses were observed post-vaccination in all of the patients. The vaccine-induced T cells had a cytotoxic phenotype and were capable of trafficking to the tumor and mediating cell killing. In addition, epitope spread to neoantigens not included in the vaccine was detected post-vaccination. These data support the safety and immunogenicity of this regimen in patients with advanced solid tumors (Clinicaltrials.gov: NCT02897765).

INTRODUCTION

The repertoire of tumor-specific T cells in cancer patients is shaped by interactions between the tumor and the host's immune response. Neoantigens, encoded by mutations that are unique to a patient's tumors, are key targets of effective anti-tumor immune responses (Hu et al., 2018; Schumacher and Schreiber, 2015). Recent first-in-human clinical trials, harnessing the ability to identify neoantigens in real time using next-generation sequencing technology and computational pipelines, have demonstrated that personalized neoantigen vaccines are feasible, safe, and immunogenic in cancer patients (Carreno et al., 2015; Hilf et al., 2019; Keskin et al., 2019; Ott et al., 2017; Sahin et al., 2017).

Immune checkpoint inhibition (ICI) has revolutionized the treatment of cancer patients over the past decade. Treatment with anti-programmed cell death 1 (PD-1) and anti-PD-1 ligand 1 (PD-L1) antibodies have demonstrated substantial anti-tumor activity in multiple tumor types (Havel et al., 2019; Yarchoan et al., 2017). Despite the success of anti-PD-1 therapy across a wide range of tumor types, only a subset of patients receives long-term clinical benefit from the treatment (Sharma and Allison, 2015). Consequently, there has been a great deal of interest in combination therapies to improve the efficacy of ICI and ultimately patient outcomes.

Neoantigens arise from mutations in cancer cells and are important targets of T cell-mediated immunity. A high

neoantigen burden in tumors is associated with favorable clinical response and improved progression-free survival (PFS) in patients with multiple tumor types treated with anti-PD-1 (Łuksza et al., 2017; McGranahan et al., 2016; Rizvi et al., 2015; Van Allen et al., 2015). Given the early promise of personalized neoantigen vaccines in the adjuvant setting (Ott et al., 2017; Sahin et al., 2017), coupled with the observation that the anti-tumor activity of PD-1 inhibition in melanoma is largely limited to patients with tumors exhibiting a preexisting T cell infiltrate (Tumeh et al., 2014), there is a strong rationale for combining these modalities in the metastatic setting. We reasoned that this strategy could augment the response rates and durability of responses over the results of PD-1 inhibition alone by inducing, expanding, and broadening the tumor-directed T cell repertoire.

We report here the first clinical trial combining a personalized neoantigen vaccine (NEO-PV-01) with PD-1 inhibition, in patients with high TMB metastatic tumors including melanoma, non-small cell lung cancer (NSCLC), and urothelial carcinoma (TCC) of the bladder (NCT02897765). In addition to addressing the feasibility and safety of this combination in a large phase Ib study, we performed comprehensive molecular and immune analyses to define the parameters associated with progression-free survival. These analyses revealed that there were few preexisting neoantigen responses. However, following vaccination, there was induction of neoantigen-specific cytotoxic T cells that can traffic to the tumor. In addition, epitope spread to non-vaccinating epitopes and major pathological responses were seen post-vaccination. The approach described here presents a treatment strategy for metastatic tumors based on increasing the frequencies of neoantigen-specific T cells to control tumor growth and spread.

RESULTS

Treatment with NEO-PV-01 Plus Anti-PD-1 Is Feasible and Safe in Metastatic Cancer Patients

The study was open to patients with unresectable or metastatic melanoma, smoking-associated NSCLC, and TCC of the bladder, who were enrolled at nine major cancer centers in the United States. The protocol specified at most one prior regimen for metastatic disease and no prior immunotherapy with anti-PD-1/PD-L1, although at the start of the study, nivolumab monotherapy was not approved for the first-line treatment of NSCLC or TCC. Enrollment was not restricted based on PD-L1 status. The major study endpoints included evaluations for safety, objective response, progression-free survival, and comprehensive immune analysis in blood and tumor (Method Details, study protocol).

To produce the personalized neoantigen vaccine NEO-PV-01, tumor mutations were first identified by whole exome and RNA sequencing of each patient's formalin-fixed tumor and matched normal cells from blood as outlined in the vaccine manufacturing schema (Figure 1A). High-quality neoepitopes encoded by somatic mutations were then selected using bioinformatics algorithms, as previously described (Abelin et al., 2017; Nielsen and Andreatta, 2016). Neoepitopes were prioritized based on the expression of mutated alleles by RNA sequencing, binding to autologous human leukocyte antigen A (HLA-A) and HLA-B, and additional variables. Details of the production, including the selection of vaccine peptides, are provided in Method Details. Each neoantigen vaccine consisted of up to 20 unique peptides, 14–35 amino acids in length, and was formulated in up to 4 distinct pools and mixed with the adjuvant poly-ICLC for administration. Patients were treated with nivolumab for 12 weeks while the vaccines were generated (Figure 1B, study schema). Starting at week 12, 1.5 mL NEO-PV-01 was administered subcutaneously into each of 4 separate, non-rotating anatomical sites per administration. Five priming and 2 booster vaccinations were administered within a 3-month period, which made up a full NEO-PV-01 course. Nivolumab was continued during both the vaccine and post-vaccine time periods.

Between November 2016 and August 2018, 82 patients were enrolled across 9 clinical sites and received at least 1 dose of nivolumab. This set was defined as the intention-to-treat (ITT) set (Figure 1C). Among these patients, 41% of melanoma, 67% of NSCLC, and 71% of bladder cancer patients had prior therapy (Table 1). Thirty-eight percent of melanoma patients had received prior immunotherapy, including ipilimumab (29%) and interferon-α (9%). Nineteen percent of bladder cancer patients had received prior immunotherapy, in all cases Bacillus Calmette-Guerin (BCG).

Of the 82 patients in the ITT set, 22 (27%) were not vaccinated for reasons that included radiographic or clinical progression (N = 11), insufficient tumor cellularity or low tumor mutational burden (N = 4), and other reasons (N = 7) (Figure 1C). Therefore, the vaccinated set included 60 patients, each of whom received at least 1 dose of vaccine (27 melanoma, 18 NSCLC, 15 bladder cancer). Of the 60 patients, 14 (23%) received the vaccine after radiographic progression on nivolumab by RECIST 1.1 criteria (6 melanoma, 4 NSCLC, and 4 bladder cancer). Although the role of pseudo-progression was considered in progressors, this is a relatively rare phenomenon with anti-PD-1 therapy alone (Hodi et al., 2018; Ott, 2018). In the vaccinated set, 30% of melanoma, 61% of NSCLC, and 73% of bladder cancer patients had prior therapy (Table 1). Eleven of the vaccinated patients had BRAF mutations (2 NSCLC and 9 melanoma) and 3 had KRAS mutations (all codon 12 and all in NSCLC). No other specific mutations (same amino acid change in the same gene) occurred in $\geq$5 patients in the study.

The primary objective of the study was to evaluate the safety and tolerability of NEO-PV-01 in combination with nivolumab (Tables S1–S3). The most common adverse events in vaccinated patients were injection-site reactions and influenza-like illness (52% and 35% of the patients, respectively). Injection site reactions typically manifested as transient, localized warmth and erythema. These events were mild (Common Terminology Criteria for Adverse Events [CTCAE] grade 1) in all cases except in 1 patient, who had a grade 2 injection site erythema. Injection site-related adverse events did not lead to NEO-PV-01 dose interruption or discontinuation for any patient (Table S2). Treatment-related events of grade $\geq$3 severity were noted for only 2 patients in the vaccinated group, with 1 case each of hypokalemia and rash, and 1 patient in the vaccinated group discontinued treatment for grade

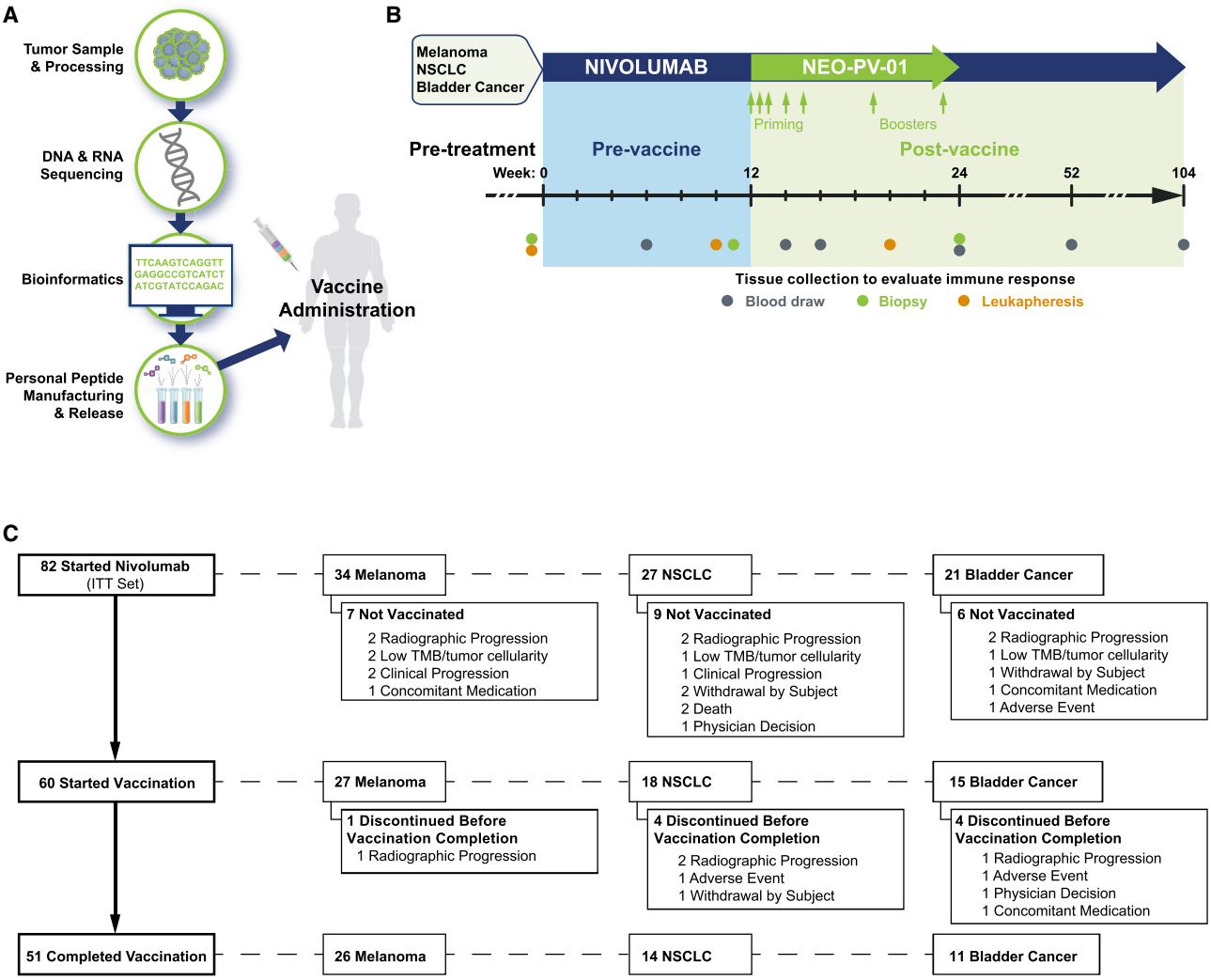

Figure 1. NEO-PV-01 Vaccine Generation, Clinical Study Design, and Patient Disposition

(A) Schematic for the sequencing of patients' tumors, prediction of neoantigens bound to class I MHC, and generation of synthetic long peptides for the personalized neoantigen vaccines.

(B) Treatment with nivolumab was initiated at week 0, NEO-PV-01 was administered between weeks 12 and 24, and nivolumab was continued for up to 2 years. Tumor biopsies and radiographic imaging were performed at weeks 0, 12, and 24 and leukaphereses were performed at the indicated time points.

(C) Study patient disposition.

2 gastritis (Table S3). No treatment-related serious adverse events were observed.

The objective response rates (ORRs, RECIST version 1.1), PFS and overall survival (OS) were analyzed with a minimum follow-up of 12 months as of the August 2019 data cutoff. Figure 2 summarizes the radiographic response profiles (RECIST 1.1) for each patient by tumor type (change in sum of target lesions) who received anti-PD-1 alone or in combination with NEO-PV-01. The pair of bar plots (top panel) for the vaccinated patients allow for the comparison of the best response before vaccine initiation (dark shade) and the best response overall (light shade). The difference indicates a further reduction in tumor size following the start of the vaccine. The PD-L1 status of the vaccinated patients did not correlate with the ORR in any of the three cohorts (Figure S1A). We note that the further tumor regression observed after vaccination could reflect delayed responses following nivolumab monotherapy, although vaccine-induced anti-tumor T cell responses may be a component of these responses. Among the vaccinated patients (N = 60), ORRs (95% confidence interval [CI]) were 59% (39%–78%), 39% (17%–64%), and 27% (8%–55%) for melanoma, NSCLC, and bladder cancer patients, respectively. The median duration of response was not reached for any of the three cohorts. Efficacy data for the ITT and the vaccinated sets are included in Table S4. Overall, 8 of 60 vaccinated patients met the criteria for tumor response conversions, for a response conversion rate (RCR) of 13%. The RCRs for the melanoma, NSCLC, and bladder cancer patient cohorts were 15%, 17%, and 7%, respectively. Among the 14 patients

Table 1. Demographics and Baseline Disease Characteristics by Cancer Type

	Melanoma		NSCLC		Bladder Cancer	
	ITT Set (N = 34)	Vaccinated Set (N = 27)	ITT Set (N = 27)	Vaccinated Set (N = 18)	ITT Set (N = 21)	Vaccinated Set (N = 15)
Male sex, %	68	70	44	39	71	67
Median age, y	60	62	66	66	67	67
M-stage, %						
M0	3	4	NA	NA	NA	NA
M1a	24	22	NA	NA	NA	NA
M1b	29	33	NA	NA	NA	NA
M1c	44	41	NA	NA	NA	NA
AJCC stage, %						
III	3	4	7	6	29	33
IV	97	96	93	94	71	67
Elevated LDH, %	38	41	NA	NA	NA	NA
Median TMB (TMB range)	267 (20–8,431)	363 (50–8,431)	185 (65–760)	221 (109–760)	142 (42–1,447)	194 (48–1,447)
PD-L1 < 1%	29	20	41	27	61	57
PD-L1 < 50%	92	90	71	64	94	93
Median tumor size (cm)	5.3	5.2	7.2	6.8	5.2	4.7
ECOG, %						
0	82	89	41	50	48	60
1	18	11	59	50	48	40
2	0	0	0	0	5	0
Prior therapy	41	30	67	61	71	73
Prior chemotherapy	0	0	67	61	67	67
Prior platinum	NA	NA	63	61	57	53
Prior immune therapy	38	30	0	0	19	20
Prior ipilimumab	29	22	NA	NA	NA	NA

In the NSCLC cohort, all of the patients had a history of smoking, 67% of NSCLC patients in the ITT and 61% of NSCLC patients in the NEO-PV-01 sets, respectively, had adenocarcinoma; the remaining NSCLC patients had squamous cell carcinoma. Among the melanoma patients, 9% of ITT and 8% of vaccinated patients previously received interferon-α. Prior immune therapy for bladder cancer patients was BCG in all cases. One bladder cancer patient was ECOG 2 at baseline, while all others were either ECOG 0 or 1. LDH levels were available from 21 and 17 patients in the ITT and vaccinated melanoma cohorts, respectively. Tumor PD-L1 levels were available from 24 and 20, 17 and 11, and 18 and 14 of the ITT and vaccinated sets in the melanoma, NSCLC, and bladder cancer cohorts, respectively. In the melanoma and bladder cohorts there were 29% and 48% smokers, respectively. AJCC, American Joint Committee on Cancer; BCG, Bacillus Calmette-Guerin; ECOG, Eastern Cooperative Oncology Group; LDH, lactate dehydrogenase; NA, not applicable.

who had progressive disease before vaccination, 1 patient with NSCLC had a partial response and 1 patient with bladder cancer experienced stable disease after vaccination.

Kaplan-Meier estimates for PFS and OS in both the ITT and vaccinated cohorts for the melanoma, NSCLC, and bladder cancer patients are shown in Figures S1B and S1C, respectively. The median PFS (95% CI) among vaccinated patients was 23.5 months (6.6, NE), 8.5 months (3.9, NE), and 5.8 months (2.8, 12.7) in the melanoma, NSCLC, and bladder cancer cohorts, respectively. The median OS for vaccinated patients was not reached in the melanoma and NSCLC cohorts, while for the bladder cancer cohort, the median OS was 20.7 months (4.8, NE). The 1-year OS rates were 96% (76%–99%), 83% (57%–94%) and 67% (38%–85%) for melanoma, NSCLC, and bladder cancer patients, respectively (Table S4). These data compare favorably with historical data for anti-PD-1 monotherapy (Balar et al., 2017; Bellmunt et al., 2017; Borghaei et al., 2015; Carbone et al., 2017; Herbst et al., 2016; Larkin et al., 2018; Schachter et al., 2017; Sharma et al., 2016; Wolchok et al., 2017). Patients with prior treatment tended to have worse PFS, as has been demonstrated with other trials testing checkpoint therapy (Borghaei et al., 2015; Herbst et al., 2016; Larkin et al., 2018). The clinical data indicate that vaccination with personalized neoantigens is feasible and safe in multiple solid tumor types when co-administered with anti-PD-1 therapy. The single-arm design of the trial does not allow attribution of responses specifically to the vaccine since it was administered in combination with anti-PD-1.

Distinct Immune and Molecular Features Are Associated with PFS across the Three Tumor Cohorts

We next investigated the presence of biomarkers that could correlate with PFS across all three tumor cohorts. For this post hoc analysis, we introduced an exploratory endpoint defined by lack of progression at 9 months (PFS-9) post-initiation of nivolumab therapy for the melanoma and the NSCLC cohorts and

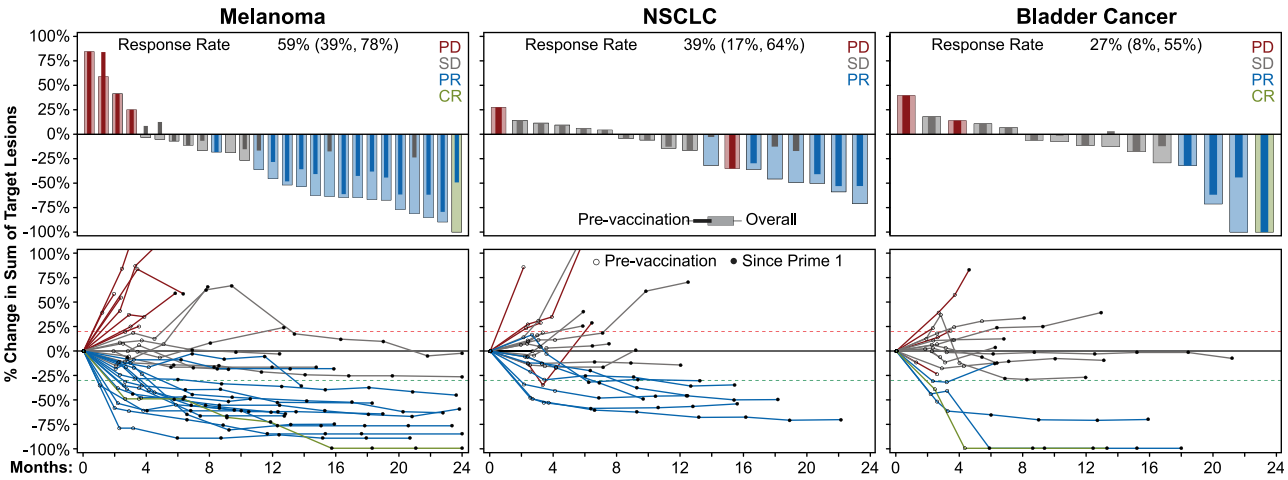

Figure 2. Rates and Durability of Responses Following Treatment with NEO-PV-01 Plus Anti-PD-1

Top: best radiographic change (%) in sum of target lesions for each patient. The dark shade narrow bars represent best change pre-NEO-PV-01; the light shade wide bars represent the overall best change in study for patients who received at least 1 dose of NEO-PV-01 plus anti-PD-1. Red indicates progressive disease, blue indicates partial response, and green indicates complete response. Bottom: radiographic changes (%) in target lesions from the initiation of nivolumab treatment for each patient. The colors are the same as in the top panel.

lack of progression at 6 months (PFS-6) for the bladder cancer cohort. Patients were classified into two groups who either did or did not achieve PFS-9 or PFS-6, respectively. The time point for bladder cancer was set at 6 months to ensure sufficient patient numbers in both groups (PFS-6 or no PFS-6, respectively) due to higher dropout in this cohort. Previous ICI monotherapy studies have investigated clinical outcomes with a variety of different markers, including tumor mutation burden (TMB) (Cristescu et al., 2018; Van Allen et al., 2015), immunological gene expression signatures in the tumor microenvironment (TME) (Ayers et al., 2017), expression of genes in the antigen presentation pathway, including β2 m (Gettinger et al., 2018; Sade-Feldman et al., 2017), and the presence of B cells and tertiary lymphoid structures in the TME (Helmink et al., 2020; Petitprez et al., 2020).

Mutational profiling of tumor by whole-exome sequencing in all ITT patients revealed a median of 215 non-silent somatic variants (Table 1). Since class I MHC expression on tumors is critical for neoepitope presentation, we also addressed the presence of β2 m mutations in tumor biopsies. There were only two patients from the ITT population who had non-silent somatic mutations in the β2 m gene, with both patients being positive for HLA class I expression on tumor cells by immunohistochemistry (IHC) (data not shown). Thus, the presence of these types of mutations was rare in the study.

With respect to TMB, we observed a significant positive correlation with PFS-9 in the melanoma cohort and a positive trend in the NSCLC cohort (Figure S2A, I). Data for the bladder cancer cohort, which had limited variability in TMB, revealed no such trend (Figure S2A, I). The epitope quality score, a unique score assigned to each candidate epitope based on its binding affinity, allele-specific expression, and proteasomal cleavage potential (Abelin et al., 2017), falls on a 0–1 scale, with higher scores corresponding to the increased likelihood of presentation. Epitope quality scores of the vaccine peptides (sum of all HLA class I epitopes in the vaccine peptides), which were correlated with overall TMB, likewise showed positive associations with PFS-9 in the melanoma and NSCLC cohorts, but only reached statistical significance for the melanoma cohort (Figure S2A, II). No association with PFS-6 was observed for the bladder cancer cohort (Figure S2A, II). Evaluation of intra-tumoral gene expression for markers of inflammation (Ayers et al., 2017) at the pre-treatment time point revealed a positive trend for the melanoma and bladder cancer cohorts, but not for the NSCLC cohort (Figure S2A, III). Data for the vaccinated set are shown in Figure S2A, panels IV, V, and VI, and, similar to the ITT set, we observed a significant positive correlation in the melanoma cohort for the epitope quality score and a trend toward positive correlation for TMB. Whole-exome sequencing of additional biopsies taken later in the treatment course showed only minor changes in the mutational landscape and TMB. Overall, these data suggest that both TMB and epitope quality are important determinants of response to the combination of the neoantigen vaccine and anti-PD-1 therapy.

To characterize potential biomarkers outside the tumor microenvironment, we evaluated distinct immune cell phenotypes including T, B, natural killer (NK), and myeloid cells in peripheral blood mononuclear cells (PBMCs) obtained at week 0 (pre-treatment), week 10 (pre-vaccine), and week 20 (post-vaccine) in patients from all 3 cohorts. Melanoma patients who achieved PFS-9 had a higher percentage of peripheral effector memory $CD8^+$ T cells compared to patients with progression before the 9-month mark, with significant differences observed at both the pre-vaccine and post-vaccine time points (Figure 3A). Conversely, the percentage of naive $CD8^+$ T cells was higher in melanoma patients with progression, with significant differences observed at all three time points (Figure 3A). Consistent with the observation of increased effector memory $CD8^+$ T cells, melanoma patients with PFS-9 had a more restricted and less diverse circulating T cell receptor (TCR) repertoire than patients who progressed (Figure 3B) (Fairfax

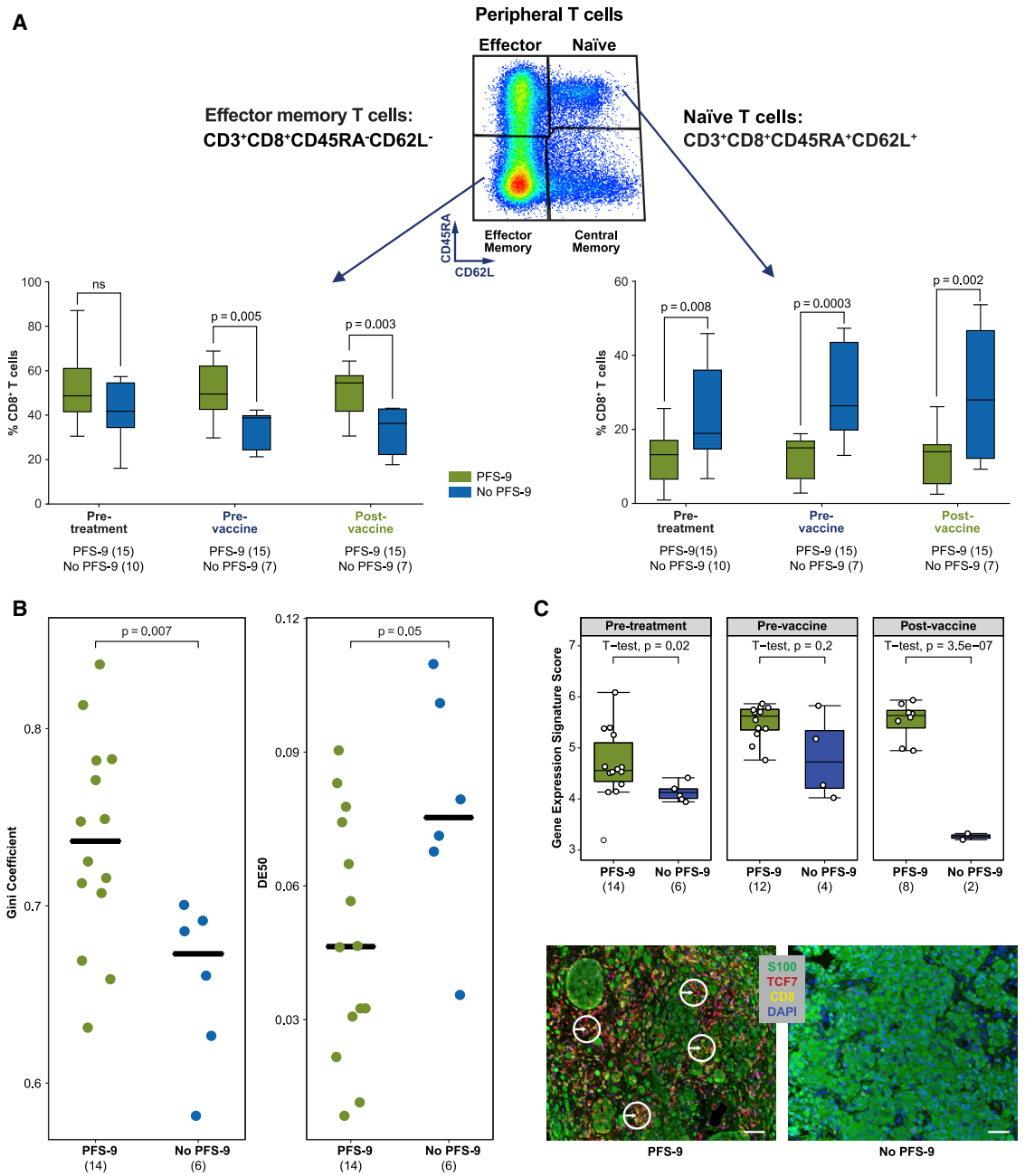

Figure 3. Increased Frequencies of Effector Memory T Cells, Increased TCR Clonality, and Presence of Tumor-Infiltrating TCF7$^+$CD8$^+$ T Cells Correlate with PFS-9 in the Melanoma Cohort

(A) Identification of peripheral effector memory and naive CD8$^+$ T cells in the melanoma cohort and correlation with PFS-9. Circulating PBMCs from pre-treatment, pre-vaccine, and post-vaccine time points were analyzed using flow cytometry to quantify effector memory and naive CD8$^+$ T cell subsets based on the expression of CD45RA and CD62L. The data are presented as box and whisker plots, with the box representing the 25th–75th percentiles, whiskers representing the minimum and maximum values, and the line represents the median. Statistical significance was determined using an unpaired t test.

(B) Measures of TCR-β diversity as observed in the PBMCs of patients with PFS-9 (green) and without PFS-9 (blue). Each dot represents 1 patient; the black horizontal bars indicate mean values. A higher Gini coefficient indicates greater skewness in clonal frequencies (i.e., higher clonality). Diversity evenness 50 (DE 50) is an alternative metric with opposite directionality.

(C) Top: expression of TCF7$^+$CD8$^+$ T cell genes in metastatic tumor biopsies of melanoma patients at pre-treatment, pre-vaccine, or post-vaccine time points using the NanoString platform. Each point represents the calculated TCF7$^+$CD8$^+$ T cell gene signature score for 1 patient. The data are presented as box and whisker plots, with the box representing the 25th–75th percentiles, the whiskers representing 1.5 times the length of the box, and the line represents the median. Statistical significance was determined using an unpaired t test. Bottom: representative images showing multiplex immunofluorescence of pre-treatment formalin-fixed paraffin-embedded (FFPE) tumor biopsies in 2 melanoma patients, 1 with PFS-9 (M7) and the other with no PFS-9 (M11), stained with DAPI (blue), CD8 (yellow), TCF7 (red), and S100 (green). The white arrows show TCF7$^+$CD8$^+$ T cell infiltrates. Scale bar, 50 μm.

et al., 2020; Hosoi et al., 2018; Kirsch et al., 2015; Thomas et al., 2013; Valpione et al., 2020).

Distinct immune phenotypes in the peripheral blood were also observed in the NSCLC and bladder cancer cohorts correlating with PFS-9 and PFS-6, respectively, although the number of samples available in these cohorts was limited. NSCLC patients who achieved PFS-9 had a lower percentage of plasmacytoid DCs than patients who progressed (Figure S2B, I). Significant correlation to plasmacytoid DCs was not seen in the melanoma or bladder cancer cohorts. Bladder cancer patients who achieved PFS-6 had a significantly higher percentage of memory $CD8^+$ T cells that was observed only at the post-vaccine time point when compared to bladder cancer patients who progressed (Figure S2B, II).

We further evaluated the presence of stem-like memory T cells in the tumor using a gene signature analysis based on recently defined genes that includes TCF7, a critical transcription factor defining stem-like T cells (Jansen et al., 2019; Sade-Feldman et al., 2018). In agreement with the memory phenotype observed in peripheral $CD8^+$ T cells of melanoma patients who had PFS-9, higher levels of stem-like memory T cell gene signatures were also seen in tumor biopsies from patients with PFS-9 compared to patients with progression (Figure 3C, upper panel). This was further corroborated by the presence of increased $CD8^+$ $TCF7^+$ T cells in the TME of patients with PFS-9 (Figure 3C, lower panel). Both the peripheral and tumor markers described above did not show changes when comparing pre-vaccine to pre-treatment samples or post-vaccine to pre-vaccine samples in patients with or without PFS-9.

We also investigated whether any germline markers correlated with PFS in each of the tumor cohorts. Notably, more melanoma patients with PFS-9 had at least one germline copy of the APOE4 genetic variant compared to patients with progression before the 9-month mark (Figure S2C) (Tavazoie et al., 2018). In contrast, an opposite correlation to the presence of the APOE4 genetic variant was seen in the NSCLC cohort and no correlation was seen in the bladder cancer patients. Further validation of these observations should be addressed in future trials.

NEO-PV-01 Plus Anti-PD1 Induces Specific and Durable T Cell Reactivity against Neoantigen Epitopes in All Tumor Cohorts

The immunogenicity of NEO-PV-01 plus nivolumab was evaluated in the peripheral blood by interferon γ (IFN-γ) ELISpot assay. Analysis of 570 vaccinating peptides across 34 patients with sufficient peripheral leukapheresis samples across all 3 time points (18 melanoma, 7 NSCLC, and 9 bladder cancer) revealed robust *de novo* immune responses to multiple vaccinating peptides in all of the patients (melanoma 52%, NSCLC 47%, and bladder cancer 52%; Figure 4A). Of these, 42% were *ex vivo* responses detected in an overnight assay with added peptide and the remainder were detected after peptide stimulation in a 5-day assay, both without added cytokines (see Method Details). Minimal neoantigen-specific T cell responses were detected at the pre-treatment and pre-vaccine time points, respectively (Figures 4A and S3A–S3C). These data are consistent with previous studies indicating that preexisting responses to neoantigens in the periphery are rarely detected (Ott et al., 2017).

Similar proportions of both $CD4^+$ and $CD8^+$ T cell responses were detected in all 3 cohorts, with an average of 42% and 24% of vaccinating peptides generating $CD4^+$ and $CD8^+$ T cell responses, respectively (Figure 4A). Specificity of the vaccine-generated immune responses to the mutant epitope versus the wild-type epitope was tested using an IFN-γ ELISpot assay across a wide range of peptide concentrations. Reactivity of the mutant versus the wild-type epitope was seen preferentially in 12 (92%) of the 13 mutant epitopes tested (Figure 4B; Table S5). Persistence of these vaccine-induced responses was tested in blood samples obtained at week 52 after the start of the anti-PD-1 treatment, or ~29 weeks after the last vaccine dose. Among the 193 neoepitopes tested in 12 melanoma, 4 NSCLC, and 4 bladder cancer patients, persistent immune responses were detected for 58% of the neoepitopes (Figure 4C). These responses included both $CD4^+$ and $CD8^+$ epitopes based on their detection in earlier (week 20) analyses. These data demonstrate that vaccination with NEO-PV-01 results in the generation of T cell responses that are specific and durable.

Neoantigen Vaccine-Specific T Cells Have Cytotoxic Potential, Migrate to the Tumor, and Can Kill Cancer Cells

Detailed phenotypic analysis of neoantigen-specific $CD4^+$ and $CD8^+$ T cell responses from selected patients with available samples revealed an activated and effector memory phenotype of these cells (Figure S4). In addition, neoantigen-specific $CD8^+$ T cells from a patient who progressed on study had higher expression of multiple co-inhibitory receptors that was not seen in the neoantigen-specific $CD4^+$ and $CD8^+$ T cells from patients who achieved PFS-9 (Figure S4). The cytotoxic phenotype of neoantigen-specific $CD4^+$ and $CD8^+$ T cells in the peripheral blood was determined by the surface expression of CD107a, a marker for T cell degranulation (Betts et al., 2003), when assayed in the presence of the neoantigen peptide. Among the 71 $CD4^+$ and $CD8^+$ T cell epitopes tested across 21 patients (13 melanoma, 3 NSCLC, and 5 bladder), the surface expression of CD107a was detected in the presence of 58% of the epitopes at the post-vaccine time point (Figures 5A and S5).

To further elucidate the role of the vaccine-induced cytolytic T cell responses in anti-tumor responses, the presence of NEO-PV-01-specific T cells was assessed by TCR sequencing in both the peripheral blood and in serial tumor biopsies from 3 melanoma patients who achieved PFS-9. Patient M1 was a 67-year-old female metastatic melanoma patient who had liver and pre-sacral metastases and experienced stable disease for 24 months on the study. A $CD8^+$ T cell response specific to a neoepitope in the RICTOR gene (IM24) was detected by tetramer analysis in PBMCs of this patient. IM24-specific $CD8^+$ T cells represented ~0.17% of all circulating $CD8^+$ T cells post-vaccine and were not present pre-vaccination (Figure 5B, I). $CD8^+$ T cells reactive to a control EBV epitope from the viral LMP2A protein were detected at all 3 time points at similar levels (~0.04% $CD8^+$ T cells; Figure S6A). Further characterization of RICTOR mutant-specific $CD8^+$ T cells revealed a memory phenotype, polyfunctionality, and cytolytic potential (Figures 5B, II, and

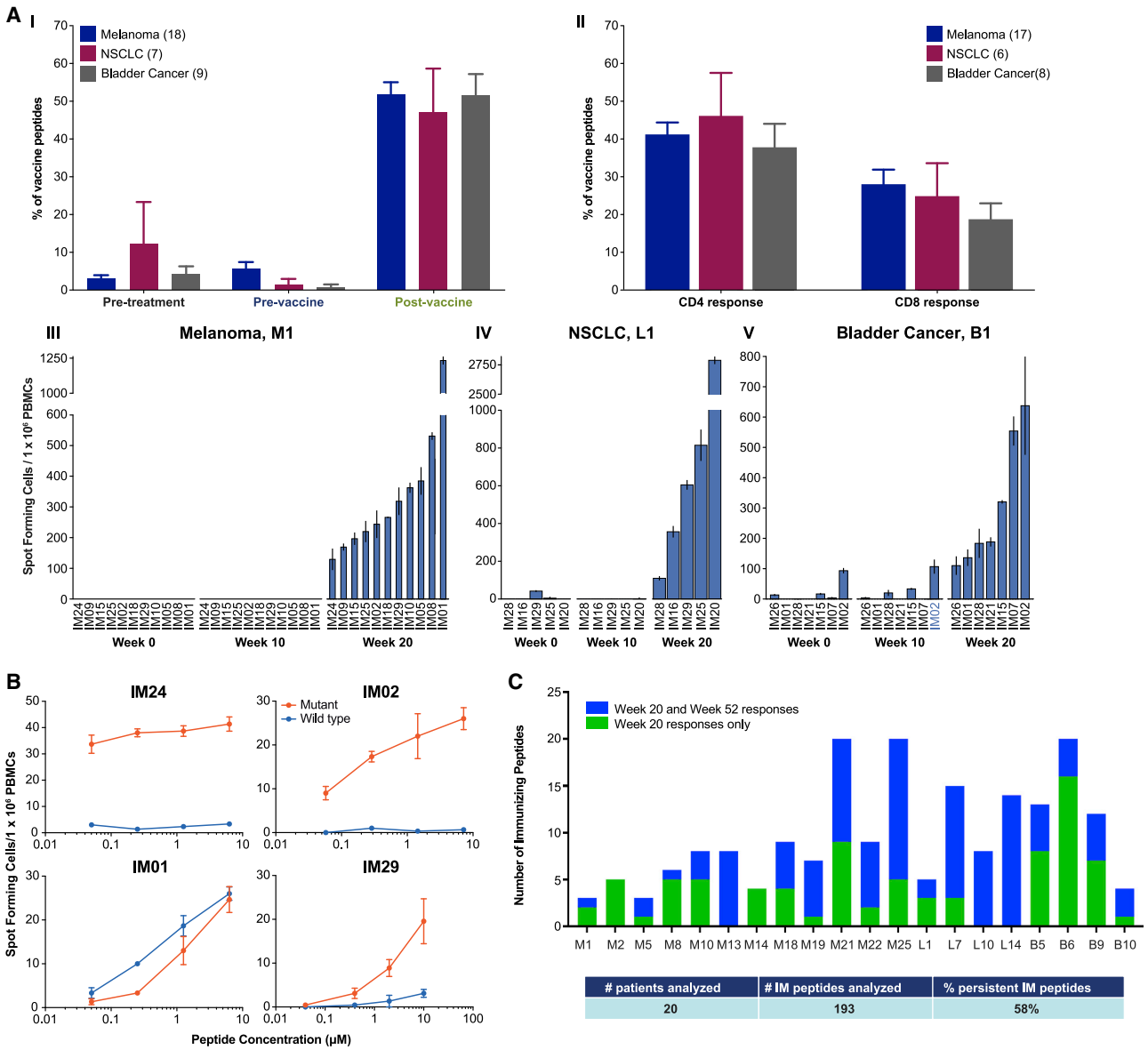

# patients analyzed	# IM peptides analyzed	% persistent IM peptides
20	193	58%

Figure 4. NEO-PV-01 Plus Anti-PD-1 Induces T Cell Reactivity against Neoantigen Epitopes That Are Mutant Specific and Persistent over Time

(A) I: percentage of all NEO-PV-01 vaccinating peptides per tumor cohort that elicited IFN-γ responses in serial PBMCs at the indicated time points as measured by IFN-γ ELISpot assay. II: percentage of $CD4^+$ versus $CD8^+$ T cell responses generated at the post-vaccine time point across all 3 tumor cohorts. III–V: deconvolution of PBMC responses to specific vaccinating peptides (immunizing [IM]) peptide measured by IFN-γ ELISpot assay in representative patients from each of the 3 tumor cohorts. Only the positive responses after background subtraction are shown. Deconvolution was done using a series of overlapping peptides for each IM peptide (Method Details). Each bar corresponds to an IM peptide and the assay peptide that generates the maximal response in either of the 2 assay formats (*ex vivo* assay or in a 5-day assay) for that IM peptide is shown. IM peptides that generated an *ex vivo* response were as follows: for melanoma patient M1—IM01, -02, -08, -18, and -24; for NSCLC patient L1—IM20, -25, -28, and -29; for bladder cancer patient B1—IM02, -07, and -28. IM peptides labeled on the x axis in blue elicited a pre-vaccine response.

(B) Specificity of immune responses as measured by *ex vivo* IFN-γ ELISpot assay to mutant peptides (red) versus wild type (blue) across a range of peptide concentrations. Representative responses from melanoma patients (IM24, IM02, and IM01) and a NSCLC (IM29) patient are depicted.

(C) Persistence of immune responses induced by IM peptides, as measured by IFN-γ ELISpot assay in PBMCs collected at week 52 after initiation of anti-PD-1 therapy. Depending on sample availability at the 52-week time point, a range of 1–20 NEO-PV-01 peptides were tested. The data are represented as stacked columns for individual patients, with responses detected at both weeks 20 and 52 (blue) and responses detected only at week 20 (green).

Aggregate data in (A) and (B) are represented as means ± SEMs.

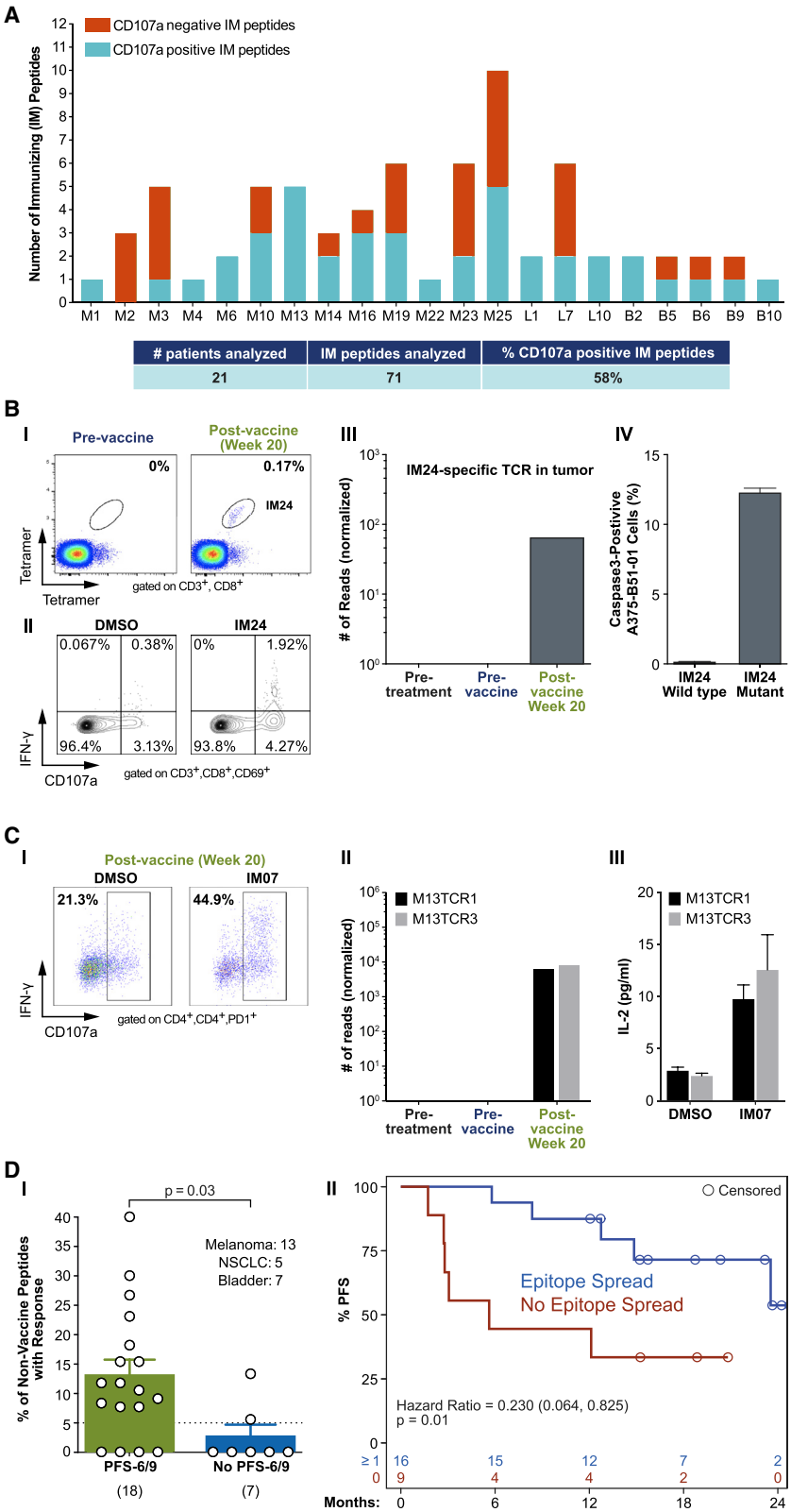

Figure 5. NEO-PV-01 Plus Anti-PD-1 Generates Cytotoxic T Cells That Can Traffic to Metastatic Tumors and Induce Epitope Spreading

(A) Cytotoxic potential of NEO-PV-01-generated immune responses as measured by the surface expression of the marker CD107a at the post-vaccine time point. A range of 1–10 NEO-PV-01 peptides were tested per patient. The data are represented as stacked columns for individual patients, with CD107a-positive responses represented in blue and CD107a-negative responses represented in red.

(B) NEO-PV-01 induced neoantigen-specific $CD8^+$ T cells are present in post-vaccine tumors of melanoma patient M1. (I) Sorting gate of IM24-$tetramer^+$ $CD8^+$ T cells present in post-vaccine PBMCs. (II) Cytotoxic potential of IM24-specific $CD8^+$ T cells as measured by the surface expression of CD107a at week 20. (III) Identification of neoantigen epitope IM24-specific TCR in the post-vaccine tumor biopsy. (IV) Cytotoxicity assay based on cleaved caspase-3 expression of A375 targets cells expressing HLA-B51:01 co-cultured with pre-treatment patient PBMCs transduced with IM24-specific TCR in the presence of mutant or wild-type IM24 peptide, respectively.

(C) Identification of neoantigen epitope IM07-specific $CD4^+$ T cells in the post-vaccine tumor of melanoma patient M13. (I) IM07-reactive $CD4^+$ T cells present in post-vaccine PBMCs. (II) Identification of IM07-specific TCRs (TCR1 and TCR3) in the post-vaccine tumor biopsy. (III) Jurkat T cells expressing the IM07-specific TCRs were co-cultured with patient antigen-presenting cells ($CD3^+$ depleted PBMCs) from the pre-treatment time point in an IL-2 secretion assay.

(D) I: Epitope spread was tested in 25 patients across all 3 tumor cohorts. Reactivity of post-vaccine PBMCs against a range of 10–19 predicted neoantigen peptides that were not included in the vaccine were tested by IFN-γ ELISpot assay in each patient. The data are presented as the percentage of non-vaccine peptides that elicited a response; each dot represents 1 patient. These responses were detected only at the post-vaccine time point. II: Kaplan-Meier plot of progression-free survival (months) by epitope spread yes (≥ 1) versus no (= 0); p value from log-rank test; hazard ratio from Cox model. The aggregate data are represented as means ± SEMs.

S6B). Single-cell sequencing of the TCR α and β chain loci was performed to identify the paired complementarity determining region 3 (CDR3) regions and revealed 3 major clones (Figure S6C). We compared the CDR3β sequences of these clones to CDR3β sequences identified by targeted sequencing of bulk RNA from serial metastatic tumors. One of these three major clones (M1TCR3) was found to be enriched in the post-vaccine tumor and was absent at the pre-treatment or pre-vaccine time points (Figure 5B, III). The sequences from M1TCR3 were cloned and expressed in the patient's pre-treatment $CD8^+$ T cells. These transduced $CD8^+$ T cells were assessed for killing of the cancer cell line A375 expressing the patient HLA allele when pulsed with either the wild-type or mutant neoepitope. Specific killing of the cancer cell line, as assessed by cleaved caspase-3 upregulation, was seen only in the presence of the mutant, but not the wild-type peptide (Figure 5B, IV).

Similarly, in patient M13, a 60-year-old male melanoma patient with lymph node metastases, who had a partial radiographic response to treatment, a functional cytolytic peripheral $CD4^+$ T cell response specific to the immunizing peptide IM07 (frameshift mutation in the gene LGALS3BP) was detected following vaccination (Figure 5C, I). Further phenotypic analysis of IM07-specific T cells demonstrated that these cells were of the memory phenotype and could secrete multiple cytokines upon stimulation with the IM07 peptide (Figure S6D). Single-cell CDR3 TCR sequence analysis of these cells revealed multiple clones (Figure S6E), of which two were detected exclusively in the post-vaccine biopsy (Figure 5C, II). Subsequent expression of M13TCRs in TCR-deficient Jurkat T cells confirmed the specificity of these TCRs for IM07 in an interleukin-2 (IL-2) secretion assay (Figure 5C, III). Cytotoxicity analysis of these IM07-specific $CD4^+$ TCRs was limited because the MHC class II restriction of these TCRs was unknown. Additional neoantigen-specific TCRs were found in the biopsies at multiple time points in 2 patients (M13 and M14) who achieved PFS-9 (Figure S6F). These data demonstrate trafficking of neoantigen-specific $CD4^+$ and $CD8^+$ T cells into the tumor.

Epitope Spread Occurs after Vaccination with NEO-PV-01 and Associates with PFS

Given the detection of memory and potentially cytolytic T cells in the tumor, we reasoned that the killing of tumor cells by neoantigen-specific T cells could release additional epitopes resulting in the generation of a broadened neoantigen-specific immune response. This phenomenon, known as epitope spreading, has been previously reported to be important for expanding the T cell responses to vaccines (Corbière et al., 2011; Kreiter et al., 2015). To assess whether epitope spread occurred after vaccination, we screened for the presence of peripheral T cell responses against epitopes that were highly ranked but were not included in the vaccine (referred to as "non-immunizing neoepitopes"). We assessed epitope spread in the two melanoma patients (patients M1 and M13) whose tumors were infiltrated with vaccine-induced neoantigen-specific T cells as assessed by single-cell TCR sequencing. Peripheral immune responses reactive against 4 of 15 and 3 of 13 non-immunizing neoepitopes were detected post-vaccination in patients M1 and M13, respectively (Figure S6G). Of note, these responses were not present pre-treatment or pre-vaccine, suggesting that the presence of epitope spread could be a surrogate marker for tumor cell killing by neoantigen-specific T cells induced by vaccination.

The presence of epitope spread was then evaluated across multiple patients with sufficient samples available for analysis. Among 330 non-immunizing neoepitopes tested across 13 melanoma, 5 NSCLC, and 7 bladder cancer patients, post-vaccine-specific immune responses were detected for 33 non-immunizing neoepitopes (Table S6). These immune responses were not detected in the pre-vaccine or pre-treatment PBMCs. Notably, the extent of epitope spread responses was higher in patients who achieved PFS-9 or PFS-6, respectively, and correlated with longer PFS across all 3 cohorts (Figure 5D). It is possible that epitope spread could be a self-amplifying process, wherein dying tumor cells can trigger additional neoantigen-specific immune responses during the course of the treatment. This was indeed the case in patient M2, a 65-year-old male melanoma patient with gastric metastases, who experienced a clinical complete response at 66 weeks from the start of treatment. An expansion of epitope spread to 3 additional non-immunizing neoepitopes was detected at 52 weeks post-initiation of anti-PD-1 therapy (Figure S6H). Thus, the observation of epitope spread suggests that NEO-PV-01-induced T cells could be cytotoxic to tumor cells and thus expand the repertoire of T cell responses against tumor neoantigens.

Major Pathological Responses (MPRs) Are Observed Post-vaccination with NEO-PV-01 in the Melanoma Cohort

The observation of epitope spread suggested that vaccination with NEO-PV-01 could lead to major changes in tumor cellularity post-vaccination. We were able to address this question in the melanoma cohort, where there were sufficient numbers of serial tumor samples available for this analysis. Tumor cellularity was evaluated in multiple longitudinal core biopsies by a blinded independent pathologist, and the highest percentage of tumor at each time point was recorded. Assessment of residual viable tumor (RVT) across the 3 longitudinal biopsies obtained from the same gastric lesion in patient M2 described above revealed the presence of considerable tumor at the pre-treatment (95%) and pre-vaccine (40%) biopsies (Figure 6A). However, there was no evidence of RVT in any of the 5 core biopsies obtained at the post-vaccine time point. Notably, increased infiltration of the tumor with $CD3^+$ T cells was seen at the pre-vaccine and post-vaccine time points (Figure 6A).

Serial tumor biopsies from 19 melanoma patients who had tumor biopsies at all 3 time points from the same anatomical site were then assessed for pathological response in relation to treatment. Of the 19 patients, 5 had tumor present at all time points. At 12 weeks after initiation of nivolumab monotherapy (pre-vaccination), 5 of 19 patients (26%) achieved MPR (RVT < 5% in all of the biopsy cores), indicating response to nivolumab monotherapy in these patients (Figure 6B, left). At 12 weeks post-initiation of vaccine, 9 melanoma patients who had not achieved an MPR with nivolumab exhibited a post-vaccine MPR (Figure 6B, right; Table S7). Three of these patients had >80% tumor pre-vaccination. We note that the MPRs seen after

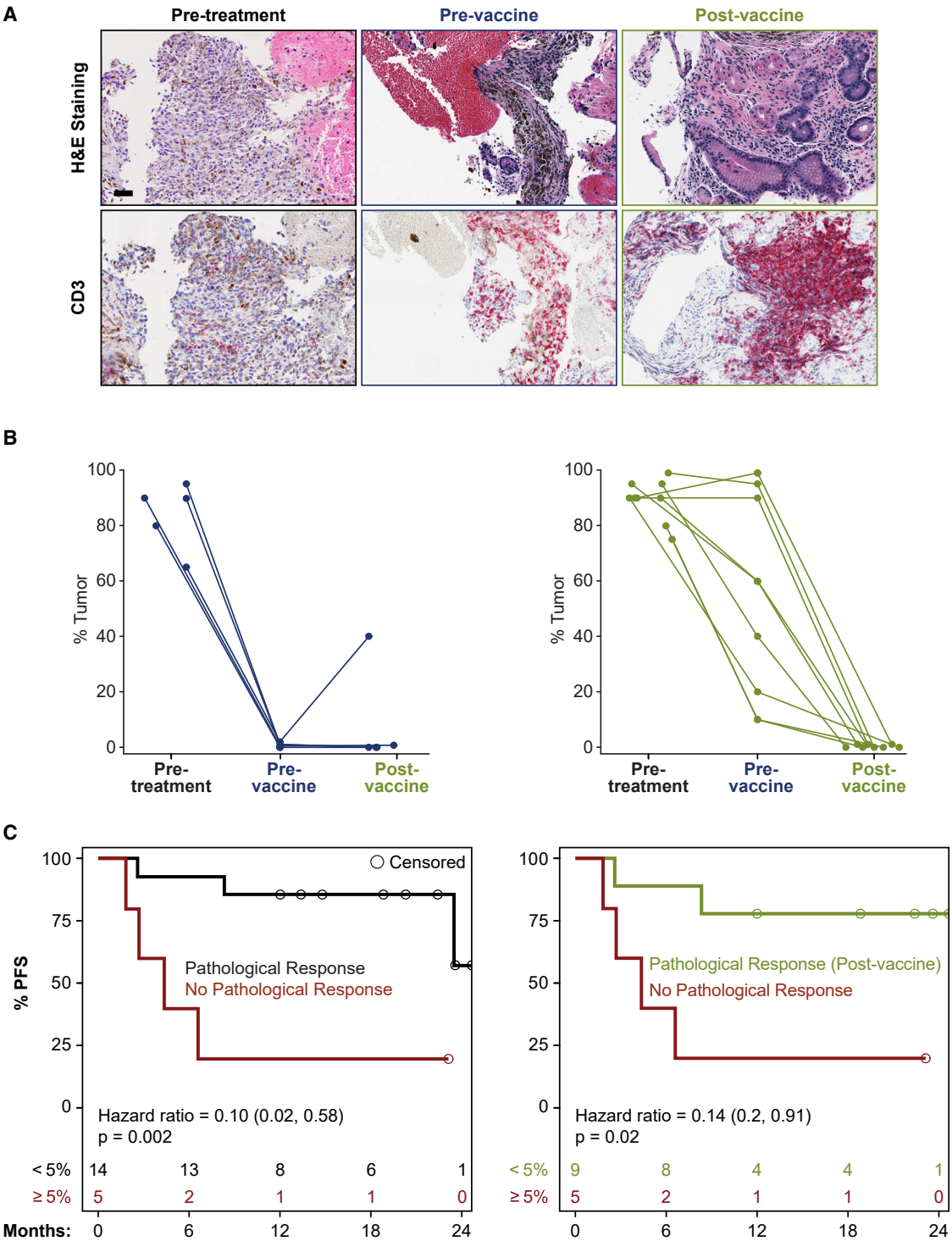

Figure 6. NEO-PV-01 Plus Anti-PD-1 Induces Major Pathological Responses (MPRs) in Patients with Residual Tumor after Initial Treatment with Anti-PD-1

(A) Representative images of H&E analysis of tumor content (top row) and anti-CD3 IHC (bottom row) from melanoma patient M2 at the indicated time points (scale bar, 50 μm).

(legend continued on next page)

vaccination could also represent delayed responses to nivolumab monotherapy. In addition, epitope spread data for 6 of the post-vaccine MPR patients were available, and 5 of them had epitope spread. Although these data are from a limited number of patients, they suggest an association of epitope spread with decreased tumor cellularity post-vaccine. Notably, all of the patients who exhibited MPR still had evidence of residual tumors by radiographic measurements, suggesting a disconnect between these measurements (3 SD, 10 PR, and 1 PD); there was no statistically significant correlation between MPR and best overall response by RESIST ($p = 0.2098$). However, the presence of MPR at any time point ($n = 14$) or seen only at the post-vaccine time point ($n = 9$) correlated with prolonged PFS compared to patients without MPR ($n = 5$; Figure 6C).

DISCUSSION

Since neoantigens are specific for tumors versus normal tissues and thus are not subject to central tolerance, they provide excellent targets for the generation and amplification of immune responses to synergize with ICI therapy (McGranahan et al., 2016; Schumacher and Schreiber, 2015). In the phase Ib trial reported here, we extend earlier studies testing personalized vaccines as monotherapy in patients with melanoma and glioblastoma multiforme (GBM) (Carreno et al., 2015; Hilf et al., 2019; Keskin et al., 2019; Ott et al., 2017; Sahin et al., 2017) by assessing the safety and feasibility of personalized neoantigen therapy in combination with anti-PD-1 therapy in the metastatic solid tumor setting. Furthermore, by studying serial tumor biopsies and PBMCs obtained pre-treatment, pre-vaccine, and post-vaccine, we were able to investigate the clinical, immune, and pathologic responses to this therapy.

We observed that radiographic responses deepened following treatment with the vaccine and were durable across all three cohorts. Of note, deepening of radiographic responses over time can be seen with nivolumab monotherapy. Comparison of all three cohorts treated with the combination of anti-PD-1 and NEO-PV-01 to historical data of anti-PD-1 monotherapy showed similar response rates, PFS, and OS (Balar et al., 2017; Bellmunt et al., 2017; Borghaei et al., 2015; Carbone et al., 2017; Herbst et al., 2016; Larkin et al., 2018; Schachter et al., 2017; Sharma et al., 2016; Wolchok et al., 2017). The relevance of such comparisons with considerably larger randomized historical clinical studies remains to be determined, as does the role of the vaccine alone.

Approximately 25% of enrolled patients were unable to proceed to vaccination, the majority due to either disease progression or inability to generate vaccines because of low tumor content in the biopsy samples or a low number of mutations. Opportunities to mitigate this issue include acceleration of vaccine production timelines and the incorporation of potentially higher-yield tumor sampling approaches. Furthermore, the selection of alternative clinical settings can be envisioned, such as the adjuvant or minimal residual disease setting or a strategy that uses pre-manufacturing of personalized vaccines at an earlier point in the disease for use during a later line of treatment.

The ability to design effective neoantigen vaccines is dependent on having a rapid computational pipeline for DNA and RNA sequence analysis and epitope scoring and prioritization. In this study, we used a mass spectrometry-based predictor (Abelin et al., 2017) to generate epitope rankings that jointly considers expression, proteasomal processing potential, and HLA-I binding affinity (Nielsen and Andreatta, 2016). This strategy yielded multiple $CD8^+$ T cell responses in the majority of the patients, but, interestingly, it also yielded frequent $CD4^+$ T cell responses despite the absence of the HLA-II binding prediction in the selection scheme. Similar observations have been made with previous neoantigen vaccines (Ott et al., 2017; Sahin et al., 2017).

A recent study by our group indicated that class II presentation is mainly dependent on the presentation of these epitopes by dendritic cells (Abelin et al., 2019). In this study, the generation of $CD4^+$ T cells is likely due to exogenous loading of peptides used in the vaccine since their size ranged from 14 to 35 amino acids, which is consistent with the length distribution of presented class II epitopes. Recent data suggest a critical role for $CD4^+$ T cells in tumor control in pre-clinical tumor models (Alspach et al., 2019; Kreiter et al., 2015). Endogenous $CD4^+$ T cell responses against neoantigens have been observed previously in patients with melanoma, and neoantigen-reactive $CD4^+$ T cells have been shown to mediate clinical regression of tumor lesions upon adoptive transfer in a patient with cholangiocarcinoma (Tran et al., 2014). In our study, we observed that post-vaccine peripheral $CD4^+$ T cells upregulated CD107a in response to stimulation with many of the vaccine neoantigen peptides, indicating their cytolytic capacity.

Another aspect of the immune responses generated by NEO-PV-01 was their phenotype and specificity. T cells generated by the vaccines exhibited a memory phenotype, had cytotoxic potential, were mutant specific and durable, and could migrate to the tumor. An interesting observation was the differential expression of co-inhibitory receptors in neoantigen-specific $CD4^+$ and $CD8^+$ T cells induced by the vaccine in patients who achieved PFS-9 or PFS-6, respectively, versus those who did not, and will require further validation. In summary, our data suggest that vaccine-induced T cells exhibited properties that would be expected in a T cell population that could mediate tumor-specific immune killing.

Epitope spread was correlated with PFS in patients across all three tumors. This observation is important for several reasons. First, it suggests that the neoantigen-induced T cells generated by NEO-PV-01 are not only capable of trafficking to the tumor but also are potentially able to kill tumor cells, leading to the release of additional neoantigens that become targets for

(B) H&E analysis of tumor content from 14 of the 19 melanoma patients who had MPR with biopsies from the same anatomical site at all 3 time points. The maximum tumor percentage seen in up to 5 cores from each biopsy site at each time point evaluated by blinded independent pathologic examination is plotted. The blue lines (left panel) illustrate MPRs at the pre-vaccine time point ($n = 5$). The green lines (right panel) illustrate MPRs at the post-vaccine time point ($n = 9$). (C) Left panel: PFS of patients with ($n = 14$) or without ($n = 5$) MPRs at any time point by Kaplan-Meier analysis. Right panel: PFS of patients with MPRs only at the post-vaccine time point ($n = 9$) or without MPR ($n = 5$) by Kaplan-Meier analysis.

additional T cells. The data suggest that it may only be necessary to target a subset of neoantigens expressed by the tumor to generate a broad immune response against the expressed neoantigens (Corbière et al., 2011). The generation of epitope spread may help to control tumor cells that do not express truncal neoantigens and thus could be a mechanism to control tumor heterogeneity.

Finally, we addressed the ability of the combination of NEO-PV-01 and anti-PD-1 to induce MPR in melanoma patients. Two patterns of MPR were noted in this analysis of 19 melanoma patients, all of whom had biopsies from the same site at all 3 time points. One group of patients (n = 5) had MPR after initial therapy with nivolumab alone. A second group of patients (n = 9) who had no or only partial pathologic responses after nivolumab, achieved MPR post-vaccination. While not directly comparable to the metastatic disease setting, given that in our study only core biopsies were examined rather than completely surgically resected disease, it is also worth noting that major or complete pathological responses were recently found to be strongly associated with superior clinical outcomes in patients with resectable stage III melanoma who received PD-1 inhibitors (Cottrell et al., 2018; Huang et al., 2019; Topalian et al., 2020) or combined PD-1 and CTLA-4 inhibitors in the neoadjuvant setting (Blank et al., 2018).

A limitation of our study is its single-arm design. Since the treatment was a combination of the neoantigen vaccine and anti-PD-1 and there was no nivolumab monotherapy comparator cohort, the deepening of radiographic responses, epitope spread, and major pathologic responses observed after vaccination cannot definitively be linked to the vaccine. Randomized trials of neoantigen-directed therapy plus anti-PD-1 versus anti-PD-1 monotherapy will be necessary to confirm these findings and determine the specific contribution of the personalized neoantigen vaccine.

In summary, we demonstrate the feasibility and safety of this personalized neoantigen-based vaccine in combination with anti-PD-1 to generate *de novo* neoantigen-specific $CD4^+$ and $CD8^+$ T cells that have a cytotoxic phenotype and are capable of trafficking to the tumor. We also observed epitope spread and evidence for major pathological responses in post-vaccination tumor biopsies. The potential to use peripheral blood and tumor biomarkers to select patients for the design of future randomized studies holds promise. These additional studies will be needed to better refine this approach and determine whether personalized neoantigen vaccines in combination with anti-PD-1 may play a role in the therapy of cancer patients.

STAR★METHODS

Detailed methods are provided in the online version of this paper and include the following:

SUPPLEMENTAL INFORMATION

Supplemental Information can be found online at https://doi.org/10.1016/j.cell.2020.08.053.

ACKNOWLEDGMENTS

We thank all of the patients and their families who participated in the study. We are grateful to all of the members of Neon Therapeutics/BioNTech US for support of and assistance in the study. We thank April Lamb and Jennifer Tepper for clinical operations; Marc Wolfgang, Scott White, Stephen Crimlisk, and Yeimy Garcia for technical operations; Jonathan McGee, Brian Sullivan, Daniel Kallin, Jeff Zhang, Amanda Aldous, and Robyn Eisert for peptide synthesis and manufacturing process development; Janani Sridar and Paul Turcott for tetramer reagent generation; Myranda Maynard and Sagar Chhangawala for bioinformatics support; Kerry Chios and John Curran for lab operation support and biobank management; and Hugh O'Dowd for support and guidance on the study. We thank Bristol-Myers Squibb for the nivolumab supply. The study was sponsored by Neon Therapeutics/BioNTech US. This manuscript is dedicated to our late colleague, Ying Sonia Ting.

AUTHOR CONTRIBUTIONS

Conceptualization and Implementation of the Study, P.A.O., L.S., R.G., E.F., and J.G. Clinical Investigators on the Study, P.A.O., S.H.-L., B.C., R.G., A.N., N.B., K.M., M.M.A., M.D.H., J.J.L., and T.F. Biomarker and Sequencing Analysis, M.E.B., K.N.B., T.E.S., A.P., D.H., Y.S.T., and M.S.R. Patient Immune Analysis, V.K., S.J.T., R.B., R.R.C., K.N.B., and B.T. TCR Sequencing and Analysis, R.B., J.S., A.P., and Y.S.T. Peptide Synthesis and Purification, J.Z.D., Y.W., and Y.H. Tetramer Reagent Generation, D.B. Informatics Support and Clinical Data Management, Z.H. and A.W. Clinical Operations and Program Management, L.D.C., M.A.M., and K.M. Biostatistics Support, J.G.

and Z.S.K. Medical Monitor on the Study, M.D. Manuscript Preparation (with input from all of the authors), P.A.O., L.S., R.B.G., M.D., Z.S.K., and M.S.R.

DECLARATION OF INTERESTS

P.A.O.: research funding paid to the institution—Bristol-Myers Squibb, Merck, AstraZeneca, Celldex, CytomX, GlaxoSmithKline, ARMO Biosciences, Neon Therapeutics; consultant—Array, Bristol-Myers Squibb, Merck, Genentech, Pfizer, Novartis, Neon Therapeutics, CytomX, Celldex.

S.H.-L.: consultant—Amgen, Bristol-Myers Squibb, Genmab, Xencor; research support—Bristol-Myers Squibb, Merck, and Vaccinex.

B.C.: member of the speakers' bureaus for Regeneron and Sanofi.

R.G.: advisory board member—Achilles; consultant—Horizon Pharma (spouse), GenePlus.

A.N.: research funding from NCI, EMD Serono, MedImmune, Healios Oncology Nutrition, Atterocor, Amplimmune, ARMO BioSciences, Eli Lilly, Karyopharm Therapeutics, Incyte, Novartis, Regeneron, Merck, Bristol-Myers Squibb, Pfizer, CytomX Therapeutics, Neon Therapeutics, Calithera Biosciences, TopAlliance Biosciences, Kymab, PsiOxus, and Immune Deficiency Foundation (spouse); advisory board member—CytomX Therapeutics, Novartis, Kymab, and Genome; travel and accommodation expense—ARMO BioSciences.

N.B.: scientific advisory board member—Checkpoint Sciences, Curevac, Primevax, Novartis, Avidea, BI, Rome Therapeutics, Neon Therapeutics, Roche, and Genentech. Extramural member of the Parker Institute for Cancer Immunotherapy

K.M.: advisory boards or consultant—Nektar, ImaginAb, Neoleukin, and Akrevia; DSMB—IOvance.

M.M.A.: research grants—Genentech, Bristol-Myers Squibb, AstraZeneca, Lilly; consultant—Genentech, Bristol-Myers Squibb, AstraZeneca, Merck, Maverick, Blueprint Medicine, Syndax, Ariad, Nektar, Gritstone, and Neon Therapeutics

M.D.H.: research funding—Bristol-Myers Squibb; consultant—Merck, Bristol-Myers Squibb, AstraZeneca, Genentech/Roche, Nektar, Syndax, Mirati, Blueprint, Immunai, and Shattuck Labs; travel support/honoraria—AstraZeneca, Eli Lilly, Merck, and Bristol-Myers Squibb; and a patent has been filed by MSK related to the use of tumor mutation burden to predict the response to immunotherapy (PCT/US2015/062208), which has received licensing fees from PGDx.

J.J.L.: honoraria/consultant—Pfizer, C4 Therapeutics, Nuvalent, and Genentech; institutional research funding—Neon, Hengrui Therapeutics, Turning Point Therapeutics, and Novartis; travel fees—Pfizer; CME funding—OncLive.

T.F.: research funding—Janssen; research funding to the institute—Seattle Genetics, Incyte, Bristol-Myers Squibb, Neon Therapeutics, and Roche/Genentech.

R.B.G.: board of directors—Alkermes plc and Infinity Pharmaceuticals; scientific advisory board—Leap Therapeutics; stockholder and employee—Neon Therapeutics/BioNTech US.

Stockholder and either current or past employees of Neon Therapeutics/BioNTech US: M.E.B., K.N.B., T.E.S., V.K., S.J.T., R.B., R.R.C., B.T., J.S., A.P., D.H., D.B., Y.S.T., J.Z.D., Y.W., Y.H., Z.H., A.W., L.D.C., M.A.M., K.M., J.G., Z.S.K., M.S.R., M.D., E.F., and L.S.

Received: March 3, 2020
Revised: May 8, 2020
Accepted: August 28, 2020
Published: October 15, 2020

REFERENCES

Abelin, J.G., Keskin, D.B., Sarkizova, S., Hartigan, C.R., Zhang, W., Sidney, J., Stevens, J., Lane, W., Zhang, G.L., Eisenhaure, T.M., et al. (2017). Mass Spectrometry Profiling of HLA-Associated Peptidomes in Mono-allelic Cells Enables More Accurate Epitope Prediction. Immunity *46*, 315–326.

Abelin, J.G., Harjanto, D., Malloy, M., Suri, P., Colson, T., Goulding, S.P., Creech, A.L., Serrano, L.R., Nasir, G., Nasrullah, Y., et al. (2019). Defining HLA-II Ligand Processing and Binding Rules with Mass Spectrometry Enhances Cancer Epitope Prediction. Immunity *51*, 766–779.e17.

Alspach, E., Lussier, D.M., Miceli, A.P., Kizhvatov, I., DuPage, M., Luoma, A.M., Meng, W., Lichti, C.F., Esaulova, E., Vomund, A.N., et al. (2019). MHC-II neoantigens shape tumour immunity and response to immunotherapy. Nature *574*, 696–701.

Aronesty, E. (2011). ea-utils: "Command-line tools for processing biological sequencing data (GitHub). https://expressionanalysis.github.io/ea-utils/.

Ayers, M., Lunceford, J., Nebozhyn, M., Murphy, E., Loboda, A., Kaufman, D.R., Albright, A., Cheng, J.D., Kang, S.P., Shankaran, V., et al. (2017). IFN-γ-related mRNA profile predicts clinical response to PD-1 blockade. J. Clin. Invest. *127*, 2930–2940.

Balar, A.V., Galsky, M.D., Rosenberg, J.E., Powles, T., Petrylak, D.P., Bellmunt, J., Loriot, Y., Necchi, A., Hoffman-Censits, J., Perez-Gracia, J.L., et al.; IMvigor210 Study Group (2017). Atezolizumab as first-line treatment in cisplatin-ineligible patients with locally advanced and metastatic urothelial carcinoma: a single-arm, multicentre, phase 2 trial. Lancet *389*, 67–76.

Banu, N., Chia, A., Ho, Z.Z., Garcia, A.T., Paravasivam, K., Grotenbreg, G.M., Bertoletti, A., and Gehring, A.J. (2014). Building and optimizing a virus-specific T cell receptor library for targeted immunotherapy in viral infections. Sci. Rep. *4*, 4166.

Bellmunt, J., de Wit, R., Vaughn, D.J., Fradet, Y., Lee, J.L., Fong, L., Vogelzang, N.J., Climent, M.A., Petrylak, D.P., Choueiri, T.K., et al.; KEYNOTE-045 Investigators (2017). Pembrolizumab as Second-Line Therapy for Advanced Urothelial Carcinoma. N. Engl. J. Med. *376*, 1015–1026.

Betts, M.R., Brenchley, J.M., Price, D.A., De Rosa, S.C., Douek, D.C., Roederer, M., and Koup, R.A. (2003). Sensitive and viable identification of antigen-specific CD8+ T cells by a flow cytometric assay for degranulation. J. Immunol. Methods *281*, 65–78.

Blair, C.K., Folsom, A.R., Knopman, D.S., Bray, M.S., Mosley, T.H., and Boerwinkle, E. (2005). APOE genotype and cognitive decline in a middle-aged cohort. Neurology *64*, 268–276.

Blank, C.U., Rozeman, E.A., Fanchi, L.F., Sikorska, K., van de Wiel, B., Kvistborg, P., Krijgsman, O., van den Braber, M., Philips, D., Broeks, A., et al. (2018). Neoadjuvant versus adjuvant ipilimumab plus nivolumab in macroscopic stage III melanoma. Nat. Med. *24*, 1655–1661.

Bolotin, D.A., Poslavsky, S., Mitrophanov, I., Shugay, M., Mamedov, I.Z., Putintseva, E.V., and Chudakov, D.M. (2015). MiXCR: software for comprehensive adaptive immunity profiling. Nat. Methods *12*, 380–381.

Borghaei, H., Paz-Ares, L., Horn, L., Spigel, D.R., Steins, M., Ready, N.E., Chow, L.Q., Vokes, E.E., Felip, E., Holgado, E., et al. (2015). Nivolumab versus Docetaxel in Advanced Nonsquamous Non-Small-Cell Lung Cancer. N. Engl. J. Med. *373*, 1627–1639.

Haas, B.J., Dobin, A., Stransky, N., Li, B., Yang, X., Tickle, T., Bankapur, A., Ganote, C., Doak, T.G., Pochet, N., Sun, J., Wu, C.J., Gingeras, T.R., and Regev, A. (2017). STAR-Fusion: Fast and Accurate Fusion Transcript Detection from RNA-Seq. bioRxiv. https://doi.org/10.1101/120295.

Carbone, D.P., Reck, M., Paz-Ares, L., Creelan, B., Horn, L., Steins, M., Felip, E., van den Heuvel, M.M., Ciuleanu, T.E., Badin, F., et al.; CheckMate 026 Investigators (2017). First-Line Nivolumab in Stage IV or Recurrent Non-Small-Cell Lung Cancer. N. Engl. J. Med. *376*, 2415–2426.

Carreno, B.M., Magrini, V., Becker-Hapak, M., Kaabinejadian, S., Hundal, J., Petti, A.A., Ly, A., Lie, W.R., Hildebrand, W.H., Mardis, E.R., and Linette, G.P. (2015). Cancer immunotherapy. A dendritic cell vaccine increases the breadth and diversity of melanoma neoantigen-specific T cells. Science *348*, 803–808.

Carter, S.L., Cibulskis, K., Helman, E., McKenna, A., Shen, H., Zack, T., Laird, P.W., Onofrio, R.C., Winckler, W., Weir, B.A., et al. (2012). Absolute quantification of somatic DNA alterations in human cancer. Nat. Biotechnol. *30*, 413–421.

Challis, D., Yu, J., Evani, U.S., Jackson, A.R., Paithankar, S., Coarfa, C., Milosavljevic, A., Gibbs, R.A., and Yu, F. (2012). An integrative variant analysis suite for whole exome next-generation sequencing data. BMC Bioinformatics *13*, 8.

Christoforides, A., Carpten, J.D., Weiss, G.J., Demeure, M.J., Von Hoff, D.D., and Craig, D.W. (2013). Identification of somatic mutations in cancer through Bayesian-based analysis of sequenced genome pairs. BMC Genomics *14*, 302.

Cibulskis, K., McKenna, A., Fennell, T., Banks, E., DePristo, M., and Getz, G. (2011). ContEst: estimating cross-contamination of human samples in next-generation sequencing data. Bioinformatics *27*, 2601–2602.

Cibulskis, K., Lawrence, M.S., Carter, S.L., Sivachenko, A., Jaffe, D., Sougnez, C., Gabriel, S., Meyerson, M., Lander, E.S., and Getz, G. (2013). Sensitive detection of somatic point mutations in impure and heterogeneous cancer samples. Nat. Biotechnol. *31*, 213–219.

Cohen, C.J., Zhao, Y., Zheng, Z., Rosenberg, S.A., and Morgan, R.A. (2006). Enhanced antitumor activity of murine-human hybrid T-cell receptor (TCR) in human lymphocytes is associated with improved pairing and TCR/CD3 stability. Cancer Res. *66*, 8878–8886.

Corbière, V., Chapiro, J., Stroobant, V., Ma, W., Lurquin, C., Lethé, B., van Baren, N., Van den Eynde, B.J., Boon, T., and Coulie, P.G. (2011). Antigen spreading contributes to MAGE vaccination-induced regression of melanoma metastases. Cancer Res. *71*, 1253–1262.

Cottrell, T.R., Thompson, E.D., Forde, P.M., Stein, J.E., Duffield, A.S., Anagnostou, V., Rekhtman, N., Anders, R.A., Cuda, J.D., Illei, P.B., et al. (2018). Pathologic features of response to neoadjuvant anti-PD-1 in resected non-small-cell lung carcinoma: a proposal for quantitative immune-related pathologic response criteria (irPRC). Ann. Oncol. *29*, 1853–1860.

Cristescu, R., Mogg, R., Ayers, M., Albright, A., Murphy, E., Yearley, J., Sher, X., Liu, X.Q., Lu, H., Nebozhyn, M., et al. (2018). Pan-tumor genomic biomarkers for PD-1 checkpoint blockade-based immunotherapy. Science *362*, eaar3593.

Fairfax, B.P., Taylor, C.A., Watson, R.A., Nassiri, I., Danielli, S., Fang, H., Mahé, E.A., Cooper, R., Woodcock, V., Traill, Z., et al. (2020). Peripheral $CD8^+$ T cell characteristics associated with durable responses to immune checkpoint blockade in patients with metastatic melanoma. Nat. Med. *26*, 193–199.

Garboczi, D.N., Hung, D.T., and Wiley, D.C. (1992). HLA-A2-peptide complexes: refolding and crystallization of molecules expressed in Escherichia coli and complexed with single antigenic peptides. Proc. Natl. Acad. Sci. USA *89*, 3429–3433.

Gettinger, S.N., Choi, J., Mani, N., Sanmamed, M.F., Datar, I., Sowell, R., Du, V.Y., Kaftan, E., Goldberg, S., Dong, W., et al. (2018). A dormant TIL phenotype defines non-small cell lung carcinomas sensitive to immune checkpoint blockers. Nat. Commun. *9*, 3196.

Havel, J.J., Chowell, D., and Chan, T.A. (2019). The evolving landscape of biomarkers for checkpoint inhibitor immunotherapy. Nat. Rev. Cancer *19*, 133–150.

Helmink, B.A., Reddy, S.M., Gao, J., Zhang, S., Basar, R., Thakur, R., Yizhak, K., Sade-Feldman, M., Blando, J., Han, G., et al. (2020). B cells and tertiary lymphoid structures promote immunotherapy response. Nature *577*, 549–555.

Herbst, R.S., Baas, P., Kim, D.W., Felip, E., Pérez-Gracia, J.L., Han, J.Y., Molina, J., Kim, J.H., Arvis, C.D., Ahn, M.J., et al. (2016). Pembrolizumab versus docetaxel for previously treated, PD-L1-positive, advanced non-small-cell lung cancer (KEYNOTE-010): a randomised controlled trial. Lancet *387*, 1540–1550.

Hilf, N., Kuttruff-Coqui, S., Frenzel, K., Bukur, V., Stevanović, S., Gouttefangeas, C., Platten, M., Tabatabai, G., Dutoit, V., van der Burg, S.H., et al. (2019). Actively personalized vaccination trial for newly diagnosed glioblastoma. Nature *565*, 240–245.

Hodi, F.S., Ballinger, M., Lyons, B., Soria, J.C., Nishino, M., Tabernero, J., Powles, T., Smith, D., Hoos, A., McKenna, C., et al. (2018). Immune-Modified Response Evaluation Criteria In Solid Tumors (imRECIST): Refining Guidelines to Assess the Clinical Benefit of Cancer Immunotherapy. J. Clin. Oncol. *36*, 850–858.

Hosoi, A., Takeda, K., Nagaoka, K., Iino, T., Matsushita, H., Ueha, S., Aoki, S., Matsushima, K., Kubo, M., Morikawa, T., et al. (2018). Increased diversity with reduced "diversity evenness" of tumor infiltrating T-cells for the successful cancer immunotherapy. Sci. Rep. *8*, 1058.

Hu, Z., Ott, P.A., and Wu, C.J. (2018). Towards personalized, tumour-specific, therapeutic vaccines for cancer. Nat. Rev. Immunol. *18*, 168–182.

Huang, A.C., Orlowski, R.J., Xu, X., Mick, R., George, S.M., Yan, P.K., Manne, S., Kraya, A.A., Wubbenhorst, B., Dorfman, L., et al. (2019). A single dose of neoadjuvant PD-1 blockade predicts clinical outcomes in resectable melanoma. Nat. Med. *25*, 454–461.

Jansen, C.S., Prokhnevska, N., Master, V.A., Sanda, M.G., Carlisle, J.W., Bilen, M.A., Cardenas, M., Wilkinson, S., Lake, R., Sowalsky, A.G., et al. (2019). An intra-tumoral niche maintains and differentiates stem-like CD8 T cells. Nature *576*, 465–470.

Keskin, D.B., Anandappa, A.J., Sun, J., Tirosh, I., Mathewson, N.D., Li, S., Oliveira, G., Giobbie-Hurder, A., Felt, K., Gjini, E., et al. (2019). Neoantigen vaccine generates intratumoral T cell responses in phase Ib glioblastoma trial. Nature *565*, 234–239.

Kirsch, I., Vignali, M., and Robins, H. (2015). T-cell receptor profiling in cancer. Mol. Oncol. *9*, 2063–2070.

Koboldt, D.C., Zhang, Q., Larson, D.E., Shen, D., McLellan, M.D., Lin, L., Miller, C.A., Mardis, E.R., Ding, L., and Wilson, R.K. (2012). VarScan 2: somatic mutation and copy number alteration discovery in cancer by exome sequencing. Genome Res. *22*, 568–576.

Kreiter, S., Vormehr, M., van de Roemer, N., Diken, M., Löwer, M., Diekmann, J., Boegel, S., Schrörs, B., Vascotto, F., Castle, J.C., et al. (2015). Mutant MHC class II epitopes drive therapeutic immune responses to cancer. Nature *520*, 692–696.

Kuball, J., Dossett, M.L., Wolfl, M., Ho, W.Y., Voss, R.H., Fowler, C., and Greenberg, P.D. (2007). Facilitating matched pairing and expression of TCR chains introduced into human T cells. Blood *109*, 2331–2338.

Lai, Z., Markovets, A., Ahdesmaki, M., Chapman, B., Hofmann, O., McEwen, R., Johnson, J., Dougherty, B., Barrett, J.C., and Dry, J.R. (2016). VarDict: a novel and versatile variant caller for next-generation sequencing in cancer research. Nucleic Acids Res. *44*, e108.

Larkin, J., Minor, D., D'Angelo, S., Neyns, B., Smylie, M., Miller, W.H., Jr., Gutzmer, R., Linette, G., Chmielowski, B., Lao, C.D., et al. (2018). Overall Survival in Patients With Advanced Melanoma Who Received Nivolumab Versus Investigator's Choice Chemotherapy in CheckMate 037: A Randomized, Controlled, Open-Label Phase III Trial. J. Clin. Oncol. *36*, 383–390.

Li, B., and Dewey, C.N. (2011). RSEM: accurate transcript quantification from RNA-Seq data with or without a reference genome. BMC Bioinformatics *12*, 323.

Li, H., and Durbin, R. (2009). Fast and accurate short read alignment with Burrows-Wheeler transform. Bioinformatics *25*, 1754–1760.

Li, H., Handsaker, B., Wysoker, A., Fennell, T., Ruan, J., Homer, N., Marth, G., Goncalo, A., and Durbin, R.; 1000 Genome Project Data Processing Subgroup (2009). The Sequence Alignment/Map format and SAMtools. Bioinformatics *25*, 2078–2079.

Łuksza, M., Riaz, N., Makarov, V., Balachandran, V.P., Hellmann, M.D., Solovyov, A., Rizvi, N.A., Merghoub, T., Levine, A.J., Chan, T.A., et al. (2017). A neoantigen fitness model predicts tumour response to checkpoint blockade immunotherapy. Nature *551*, 517–520.

McGranahan, N., Furness, A.J., Rosenthal, R., Ramskov, S., Lyngaa, R., Saini, S.K., Jamal-Hanjani, M., Wilson, G.A., Birkbak, N.J., Hiley, C.T., et al. (2016). Clonal neoantigens elicit T cell immunoreactivity and sensitivity to immune checkpoint blockade. Science *351*, 1463–1469.

McKenna, A., Hanna, M., Banks, E., Sivachenko, A., Cibulskis, K., Kernytsky, A., Garimella, K., Altshuler, D., Gabriel, S., Daly, M., and DePristo, M.A. (2010). The Genome Analysis Toolkit: a MapReduce framework for analyzing next-generation DNA sequencing data. Genome Res. *20*, 1297–1303.

Nielsen, M., and Andreatta, M. (2016). NetMHCpan-3.0; improved prediction of binding to MHC class I molecules integrating information from multiple receptor and peptide length datasets. Genome Med. *8*, 33.

Ott, P.A. (2018). Immunotherapy: Immune-modified response criteria - an iterative learning process? Nat. Rev. Clin. Oncol. *15*, 267–268.

Ott, P.A., Hu, Z., Keskin, D.B., Shukla, S.A., Sun, J., Bozym, D.J., Zhang, W., Luoma, A., Giobbie-Hurder, A., Peter, L., et al. (2017). An immunogenic personal neoantigen vaccine for patients with melanoma. Nature *547*, 217–221.

Petitprez, F., de Reyniès, A., Keung, E.Z., Chen, T.W., Sun, C.M., Calderaro, J., Jeng, Y.M., Hsiao, L.P., Lacroix, L., Bougoüin, A., et al. (2020). B cells are associated with survival and immunotherapy response in sarcoma. Nature *577*, 556–560.

Rimmer, A., Phan, H., Mathieson, I., Iqbal, Z., Twigg, S.R.F., Wilkie, A.O.M., McVean, G., and Lunter, G.; WGS500 Consortium (2014). Integrating mapping-, assembly- and haplotype-based approaches for calling variants in clinical sequencing applications. Nat. Genet. *46*, 912–918.

Rizvi, N.A., Hellmann, M.D., Snyder, A., Kvistborg, P., Makarov, V., Havel, J.J., Lee, W., Yuan, J., Wong, P., Ho, T.S., et al. (2015). Cancer immunology. Mutational landscape determines sensitivity to PD-1 blockade in non-small cell lung cancer. Science *348*, 124–128.

Rodenko, B., Toebes, M., Hadrup, S.R., van Esch, W.J., Molenaar, A.M., Schumacher, T.N., and Ovaa, H. (2006). Generation of peptide-MHC class I complexes through UV-mediated ligand exchange. Nat. Protoc. *1*, 1120–1132.

Sade-Feldman, M., Jiao, Y.J., Chen, J.H., Rooney, M.S., Barzily-Rokni, M., Eliane, J.P., Bjorgaard, S.L., Hammond, M.R., Vitzthum, H., Blackmon, S.M., et al. (2017). Resistance to checkpoint blockade therapy through inactivation of antigen presentation. Nat. Commun. *8*, 1136.

Sade-Feldman, M., Yizhak, K., Bjorgaard, S.L., Ray, J.P., de Boer, C.G., Jenkins, R.W., Lieb, D.J., Chen, J.H., Frederick, D.T., Barzily-Rokni, M., et al. (2018). Defining T Cell States Associated with Response to Checkpoint Immunotherapy in Melanoma. Cell *175*, 998–1013.e20.

Sahin, U., Derhovanessian, E., Miller, M., Kloke, B.P., Simon, P., Löwer, M., Bukur, V., Tadmor, A.D., Luxemburger, U., Schrörs, B., et al. (2017). Personalized RNA mutanome vaccines mobilize poly-specific therapeutic immunity against cancer. Nature *547*, 222–226.

Saunders, C.T., Wong, W.S., Swamy, S., Becq, J., Murray, L.J., and Cheetham, R.K. (2012). Strelka: accurate somatic small-variant calling from sequenced tumor-normal sample pairs. Bioinformatics *28*, 1811–1817.

Schachter, J., Ribas, A., Long, G.V., Arance, A., Grob, J.J., Mortier, L., Daud, A., Carlino, M.S., McNeil, C., Lotem, M., et al. (2017). Pembrolizumab versus ipilimumab for advanced melanoma: final overall survival results of a multicentre, randomised, open-label phase 3 study (KEYNOTE-006). Lancet *390*, 1853–1862.

Schneider, C.A., Rasband, W.S., and Eliceiri, K.W. (2012). NIH Image to ImageJ: 25 years of image analysis. Nature Methods *9*, 671–675.

Schumacher, T.N., and Schreiber, R.D. (2015). Neoantigens in cancer immunotherapy. Science *348*, 69–74.

Sharma, P., and Allison, J.P. (2015). The future of immune checkpoint therapy. Science *348*, 56–61.

Sharma, P., Callahan, M.K., Bono, P., Kim, J., Spiliopoulou, P., Calvo, E., Pillai, R.N., Ott, P.A., de Braud, F., Morse, M., et al. (2016). Nivolumab monotherapy in recurrent metastatic urothelial carcinoma (CheckMate 032): a multicentre, open-label, two-stage, multi-arm, phase 1/2 trial. Lancet Oncol. *17*, 1590–1598.

Signorell, A., Aho, K.A., Alfons, A., Anderegg, N., Aragon, T., Arppe, A., Baddeley, A., Barton, K., Bolker, B., Borchers, H.W., et al. (2016). DescTools: tools for descriptive statistics. https://rdrr.io/cran/DescTools/man/DescTools-package.html.

Tavazoie, M.F., Pollack, I., Tanqueco, R., Ostendorf, B.N., Reis, B.S., Gonsalves, F.C., Kurth, I., Andreu-Agullo, C., Derbyshire, M.L., Posada, J., et al. (2018). LXR/ApoE Activation Restricts Innate Immune Suppression in Cancer. Cell *172*, 825–840.e18.

Thomas, P.G., Handel, A., Doherty, P.C., and La Gruta, N.L. (2013). Ecological analysis of antigen-specific CTL repertoires defines the relationship between naive and immune T-cell populations. Proc. Natl. Acad. Sci. USA *110*, 1839–1844.

Toebes, M., Coccoris, M., Bins, A., Rodenko, B., Gomez, R., Nieuwkoop, N.J., van de Kasteele, W., Rimmelzwaan, G.F., Haanen, J.B., Ovaa, H., and Schumacher, T.N. (2006). Design and use of conditional MHC class I ligands. Nat. Med. *12*, 246–251.

Topalian, S.L., Taube, J.M., and Pardoll, D.M. (2020). Neoadjuvant checkpoint blockade for cancer immunotherapy. Science *367*, eaax0182.

Tran, E., Turcotte, S., Gros, A., Robbins, P.F., Lu, Y.C., Dudley, M.E., Wunderlich, J.R., Somerville, R.P., Hogan, K., Hinrichs, C.S., et al. (2014). Cancer immunotherapy based on mutation-specific CD4+ T cells in a patient with epithelial cancer. Science *344*, 641–645.

Tumeh, P.C., Harview, C.L., Yearley, J.H., Shintaku, I.P., Taylor, E.J., Robert, L., Chmielowski, B., Spasic, M., Henry, G., Ciobanu, V., et al. (2014). PD-1 blockade induces responses by inhibiting adaptive immune resistance. Nature *515*, 568–571.

Valpione, S., Galvani, E., Tweedy, J., Mundra, P.A., Banyard, A., Middlehurst, P., Barry, J., Mills, S., Salih, Z., Weightman, J., et al. (2020). Immune-awakening revealed by peripheral T cell dynamics after one cycle of immunotherapy. Nat. Can. *1*, 210–221.

Van Allen, E.M., Miao, D., Schilling, B., Shukla, S.A., Blank, C., Zimmer, L., Sucker, A., Hillen, U., Foppen, M.H.G., Goldinger, S.M., et al. (2015). Genomic correlates of response to CTLA-4 blockade in metastatic melanoma. Science *350*, 207–211.

Wang, C., Sanders, C.M., Yang, Q., Schroeder, H.W., Jr., Wang, E., Babrzadeh, F., Gharizadeh, B., Myers, R.M., Hudson, J.R., Jr., Davis, R.W., and Han, J. (2010). High throughput sequencing reveals a complex pattern of dynamic interrelationships among human T cell subsets. Proc. Natl. Acad. Sci. USA *107*, 1518–1523.

Wickham, H. (2016). ggplot2: Elegant Graphics for Data Analysis (Springer).

Wolchok, J.D., Chiarion-Sileni, V., Gonzalez, R., Rutkowski, P., Grob, J.J., Cowey, C.L., Lao, C.D., Wagstaff, J., Schadendorf, D., Ferrucci, P.F., et al. (2017). Overall Survival with Combined Nivolumab and Ipilimumab in Advanced Melanoma. N. Engl. J. Med. *377*, 1345–1356.

Yarchoan, M., Hopkins, A., and Jaffee, E.M. (2017). Tumor Mutational Burden and Response Rate to PD-1 Inhibition. N. Engl. J. Med. *377*, 2500–2501.

STAR★METHODS

KEY RESOURCES TABLE

REAGENT or RESOURCE	SOURCE	IDENTIFIER
Antibodies		
Active-caspase 3-BV650	BD Biosciences	Cat # 564096; RRID:AB_2738589
Arginase-PE	R&D Systems	Cat # IC5868P
CD107a-BV786	BD Biosciences	Cat # 563869; RRID:AB_2738458
CD11b-PerCPCy5.5	BioLegend	Cat # 301328; RRID:AB_10933428
CD11c-BV510	BD Biosciences	Cat # 563026; RRID:AB_2737960
CD123-BV786	BD Biosciences	Cat # 564196; RRID:AB_2738662
CD137-BV650	BD Biosciences	Cat # 564092; RRID:AB_2738586
CD14-BUV805	BD Biosciences	Cat # 565780
CD14-FITC	BD Biosciences	Cat # 340682; RRID:AB_400086
CD141-BV711	BD Biosciences	Cat # 563155; RRID:AB_2738033
CD15-BUV396	BD Biosciences	Cat # 563872; RRID:AB_2738461
CD152 (CTLA-4)-BV421	BD Biosciences	Cat # 562743; RRID:AB_2737762
CD152 (CTLA-4)-PE Cy5	BD Biosciences	Cat # 555854; RRID:AB_396177
CD154 (CD40L)-FITC	BD Biosciences	Cat # 555699; RRID:AB_396049
CD16-FITC	BD Biosciences	Cat # 340704; RRID:AB_400104
CD16-PECy7	BD Biosciences	Cat # 557744; RRID:AB_396850
CD19-BUV496	BD Biosciences	Cat # 564655; RRID:AB_2744311
CD19-FITC	BioLegend	Cat # 555412; RRID:AB_395812
CD19-FITC	BD Biosciences	Cat # 340864; RRID:AB_400152
CD19-APCCy7	BD Biosciences	Cat # 557791; RRID:AB_396873
CD1c-BV421	BD Biosciences	Cat # 565050; RRID:AB_2744319
CD223 (LAG-3)-BV786	BioLegend	Cat # 369322; RRID:AB_2716127
CD25-BV605	BD Biosciences	Cat # 562660; RRID:AB_2744343
CD25-PerCPCy5.5	BD Biosciences	Cat # 560503; RRID:AB_1727453
CD26-APC	BioLegend	Cat # 302710; RRID:AB_10916120
CD26-PECF594	BD Biosciences	Cat # 565158; RRID:AB_2739085
CD27-BV605	BD Biosciences	Cat # 562655; RRID:AB_2744351
CD27-BV711	BD Biosciences	Cat # 356430; RRID:AB_2650751
CD3	Biocare Medical	Cat # ACI 3152A
CD3-BUV805	BD Biosciences	Cat # 565511; RRID:AB_2739275
CD3-FITC	BioLegend	Cat # 300306; RRID:AB_314042
CD3-BV421	BD Biosciences	Cat # 563797; RRID:AB_2744383
CD303-AF700	BioLegend	Cat # 354228; RRID:AB_2629744
CD33-PECy5	BD Biosciences	Cat # 551377; RRID:AB_394173
CD366 (Tim-3)-BV510	BioLegend	Cat # 345030; RRID:AB_2565831
CD4-BV711	BD Biosciences	Cat # 563028; RRID:AB_2737961
CD4-FITC	BD Biosciences	Cat # 347413; RRID:AB_400297
CD4-BV510	BD Biosciences	Cat # 562971; RRID:AB_2744424
CD4-BUV496	BD Biosciences	Cat # 564652; RRID:AB_2744422
CD45RA-Alexa Fluor 700	BD Biosciences	Cat # 560673; RRID:AB_1727496
CD45RO-PerCP Cy5.5	BD Biosciences	Cat # 560607; RRID:AB_1727500
CD45RO-BV605	BD Biosciences	Cat # 562791; RRID:AB_2744411
CD56-FITC	BioLegend	Cat # 362546; RRID:AB_2565964

(*Continued on next page*)

Continued

REAGENT or RESOURCE	SOURCE	IDENTIFIER
CD62L-FITC	BD Biosciences	Cat # 555543; RRID:AB_395927
CD69-PE Cy7	BD Biosciences	Cat # 557745; RRID:AB_396851
CD69-BV786	BD Biosciences	Cat # 563834; RRID:AB_2738441
CD8-PE Cy5	BD Biosciences	Cat # 555636; RRID:AB_395998
CD8-Alexa Fluor 700	BioLegend	Cat # 344724; RRID:AB_2562790
CD8-BUV805	BD Biosciences	Cat # 564912; RRID:AB_2744465
CD8	Biocare Medical	Cat # CRM311A
CLEC9A-AF647	BD Biosciences	Cat # 564267; RRID:AB_2738717
CTLA-4-PECy5	BD Biosciences	Cat # 555854; RRID:AB_396177
Foxp3-PE Cy7	Life Technologies	Cat # 25-4776-42; RRID:AB_10804638
Gamma-9-APC	BioLegend	Cat # 331310; RRID:AB_2057504
HLA-DR-BV650	BD Biosciences	Cat # 564231; RRID:AB_2738685
HLA-DR-BV711	BD Biosciences	Cat # 563696; RRID:AB_2738378
HLA-DR-BV650	BioLegend	Cat # 307650; RRID:AB_2563828
ICOS-BUV395	BD Biosciences	Cat # 564777; RRID:AB_2738946
IFNγ-PE	Life Technologies	Cat # 12-7319-42; RRID:AB_1311247
IFNγ-Alexa Fluor 700	eBioscience	Cat # 56-7319-42; RRID:AB_2574509
IL-10-PE-Cy7	eBioscience	Cat # 25-7108-42; RRID:AB_2573524
IL-12-BV421	BD Biosciences	Cat # 565023; RRID:AB_2739045
IL-2-PE-CF495	BD Biosciences	Cat # 562384; RRID:AB_11154601
IL-4-BV711	BD Biosciences	Cat # 564112; RRID:AB_2738600
IL-6-PerCP-e710	eBioscience	Cat # 46-7069-42; RRID:AB_11151511
LIVE/DEAD Fixable Near-IR Dead Cell Stain Kit	ThermoFisher	Cat # L10119
PD-1-PE-CF594	Invitrogen	Cat # 61-2799-42; RRID:AB_2574598
PD-1-BV510	BD Biosciences	Cat # 563076; RRID:AB_2737990
S100	Biocare Medical	Cat # CM089A
TCF7	Cell Signal Technology	Cat # 2203T
TCF7-PE	BD Biosciences	Cat # 564217; RRID:AB_2687845
TNFα-BUV395	BD Biosciences	Cat # 563996; RRID:AB_2738533
Streptavidin-PE	BioLegend	Cat # 405203
Streptavidin-BUV395	BD Biosciences	Cat # 564176
Streptavidin-APC	BioLegend	Cat # 405207
Streptavidin-BV421	BioLegend	Cat # 405225
Streptavidin-BV650	BD Biosciences	Cat # 563855
Streptavidin-Qdot 605	Life Technologies	Cat # Q10101MP
Streptavidin-Qdot 705	Life Technologies	Cat # Q10161MP
TSA-Cy3	Akoya Biosciences	Cat # NEL744001KT
TSA-Cy5	Akoya Biosciences	Cat # NEL745001KT
TSA-Fluorescein	Akoya Biosciences	Cat # NEL741001KT
ImPRESS HRP Anti-Mouse IgG (Peroxidase) Polymer Detection Kit	Vector Laboratories	Cat # MP-7402
ImPRESS HRP Anti-Rabbit IgG (Peroxidase) Polymer Detection Kit	Vector Laboratories	Cat # ML-7401
Bacterial and Virus Strains		
BL21 (DE3) Competent *E. coli*	NEB	Cat # C2527I

(*Continued on next page*)

Continued

REAGENT or RESOURCE	SOURCE	IDENTIFIER
Biological Samples		
Patient PBMCs from NT-001 trial	This manuscript	N/A
Patient Tumor Biopsies from NT-001 trial	This manuscript	N/A
Healthy Donor PBMCs	Precision for Medicine	Cat # 93000-10M
Healthy Donor PBMCs	StemExpress	Cat # LE010F
Chemicals, Peptides, and Recombinant Proteins		
CEF viral peptide pool	JPT	Cat # PM-CEF-E
Cell Stimulation Cocktail	Life Technologies	Cat # 00-4970-93
Dasatinib	Sigma-Aldrich	Cat # CDS023389
Benzonase	Millipore Sigma	Cat # 70746
d-biotin solution	AVIDITY	Cat # BIO200
Assay peptides used in Immune Analysis	This manuscript	Table S8
MHC class I tetramers	This manuscript	N/A
Critical Commercial Assays		
AEC substrate-chromogen	BD Biosciences	Cat # 551951
AllPrep DNA/RNA FFPE kit	QIAGEN	Cat # 80234
Fixation/Permeabilization Solution Kit	BD Biosciences	Cat # 554714
Foxp3/Transcription Factor Staining Buffer Set	eBioscience	Cat # 00-5523-00
Intracellular Fixation and Permeabilization Buffer Set	eBioscience	Cat # 88-8824-00
GolgiStop	BD Biosciences	Cat # 554724
GolgiPlug	BD Biosciences	Cat # 555029
IFN gamma Human ELISPOT Kit	Invitrogen	Cat # 88-7386-88
U-Plex development pack, 10-assay sector plate	Meso Scale Discovery	Cat # K15235N
Meso Scale Discovery (MSD) Read Buffer T (4x)	Meso Scale Discovery	Cat # R92TC
Meso Scale Discovery (MSD) U-Plex System	Meso Scale Discovery	Cat # K15067L
Qubit RNA HS Assay Kit	ThermoFisher	Cat # Q32855
RNA 6000 Nano Kit	Agilent	Cat # 5067-1511
RNA 6000 Pico Kit	Agilent	Cat # 5067-1513
RNeasy Plus Micro Kit	QIAGEN	Cat # 74034
RNeasy Plus Mini Kit	QIAGEN	Cat # 74134
Fixation/Permeabilization Solution Kit	BD Biosciences	Cat # 554714
Foxp3/Transcription Factor Staining Buffer Set	eBioscience	Cat # 00-5523-00
CD3 MicroBeads, human	Miltenyi Biotec	Cat # 130-050-101
CD4 MicroBeads, human	Miltenyi Biotec	Cat # 130-045-101
Pan T cell Isolation Kit, human	Miltenyi Biotec	Cat # 130-096-535
Opal 7-Color Manual IHC Kit	PerkinElmer	Cat # NEL811001KT
TSA Plus Fluorescence kit	PerkinElmer	Cat # NEL741001KT
Experimental Models: Cell Lines		
Jurkat, Clone E6-1	ATCC	Cat # ATCC-TIB-152
A375	ATCC	Cat # ATCC-CRL-1619
293FT Cell Line	Thermo Fisher	Cat # R70007

(*Continued on next page*)

Continued

REAGENT or RESOURCE	SOURCE	IDENTIFIER
Recombinant DNA		
pET-22b(+) DNA - Novagen	Millipore Sigma	Cat # 69744-3
Software and Algorithms		
R (version 3.5.1)	CRAN	https://www.r-project.org/
ImageJ	Schneider et al., 2012	https://imagej.nih.gov/ij/
FlowJo (version 10)	FlowJo Software (for Windows) Version 10. Becton, Dickinson and Company; 2019.	https://www.flowjo.com/
IPD-IMGT/HLA	N/A	https://www.ebi.ac.uk/ipd/imgt/hla
GraphPad Prism (version 7.01)	GraphPad Software, La Jolla California, USA	https://www.graphpad.com:443
BWA-MEM (version 0.7.13)	Li and Durbin, 2009	N/A
STAR-Fusion (version 2.5.1.b)	Haas et al., 2017	N/A
GATK 3.5 workflow	McKenna et al., 2010	N/A
ConTest	Cibulskis et al., 2011	N/A
VarDict (version 1.4.6)	Lai et al., 2016	N/A
Strelka (version 1.0.15)	Saunders et al., 2012	N/A
VarScan2 (version 2.3.9)	Koboldt et al., 2012	N/A
Atlas Indel2 (version 1.4.3)	Challis et al., 2012	N/A
Seurat (version 2.6)	Christoforides et al., 2013	N/A
Platypus (version 0.8.1)	Rimmer et al., 2014	N/A
RSEM (version 1.2.31)	Li and Dewey, 2011	N/A
NetMHCpan (version 3.0)	Nielsen and Andreatta, 2016	N/A
MiXCR (version 3.0.12)	Bolotin et al., 2015	N/A
DescTools package	Signorell et al., 2016	N/A
nSolver Analysis Software (version 3.0)	NanoString	https://www.nanostring.com/products/analysis-software/nsolver

RESOURCE AVAILABILITY

Lead Contact

Further information and requests for resources and reagents should be directed to and will be fulfilled by the Lead Contact, Lakshmi Srinivasan (lakshmi.srinivasan@biontech.us).

Materials Availability

All unique/stable reagents generated in this study are available from the Lead Contact with a completed Materials Transfer Agreement.

Data and Code Availability

All vaccine peptide and immune assay peptide sequences are provided in Table S8. Patient sequencing information will be provided for patients consistent with their institutional informed consent. Epitope selection utilized previously published algorithms and methods as described in the STAR Methods.

EXPERIMENTAL MODEL AND SUBJECT DETAILS

Study design

Details of the study can be found in the attached clinical study protocol NT-001 and patient demographics can be found in Table 1. Nine clinical sites enrolled patients including Dana Farber Cancer Institute, City of Hope National Medical Center, Icahn School of Medicine at Mount Sinai, Massachusetts General Hospital, Memorial Sloan Kettering Cancer Center, University of California Los Angeles, University of California San Francisco, University of Texas MD Anderson Cancer Center and Washington University School of Medicine. Patients who were 18 years of age or older with histologically or cytologically confirmed unresectable or metastatic

melanoma, NSCLC or UC of the bladder, urethra, ureter or renal pelvis were eligible for enrollment in this multicenter phase I clinical trial (NCT02897765, also known as NT001). No statistical methods were used to pre-determine the sample size for each of the three tumor cohorts. The study was conducted in accordance with the Declaration of Helsinki and with approval by the Institutional Review Board at each participating site and written informed consent was obtained for all patients. Key eligibility criteria included an Eastern Cooperative Oncology Group (ECOG) performance status of 0 or 1 and life expectancy of at least 6 months. Excluded from the study were patients with untreated central nervous system (CNS) metastases, active or history of autoimmune disease, and patients who had received previous therapy with ICI other than cytotoxic T lymphocyte-associated antigen 4 (CTLA-4) inhibition for melanoma and intra-vesical BCG for urothelial carcinoma.

The primary objective of the study was to evaluate safety of administering NEO-PV-01 + adjuvant (poly-ICLC) with nivolumab. The relationship of an adverse event to study treatments was determined according to clinical judgement of the clinical investigators. The secondary objective was to determine the anti-tumor activity of the combination as assessed by objective response rate and the exploratory objective was to determine the vaccine induced immune responses. The clinical characteristics for these patients are included in Table 1. NEO-PV-01 is a personalized vaccine composed of up to 20 synthesized peptides that are between 14 and 35 amino acids in length. The peptides are divided into up to four individual pools, each pool consisting of 1 to 5 peptides. On the day of vaccination, each pool of NEO-PV-01 was mixed with the adjuvant polyinosinic polycytidylic acid polylysine carboxymethylcellulose (poly ICLC; Hiltonol®) for a concentration of 300 μg/mL of each peptide. Each patient was scheduled to receive 5 doses of vaccination during the priming phase (on days 1 and 4 of week 12) and then weekly for 3 weeks (weeks 13, 14, and 15), followed by 2 booster vaccinations at weeks 19 and 23. Each pool was administered by subcutaneous injection in one of the four limbs or left or right midriff as alternative anatomical locations. The anatomical site of injection for each pool was constant through the vaccination regimen. Patients were allowed to start vaccination with NEO-PV-01 + adjuvant poly-ICLC regardless of disease status. Nivolumab at 240 mg flat dose was administered i.v. every 2 weeks starting on study day 1.

Clinical assessments

Adverse events, laboratory values, ECG, and vital signs were assessed regularly and graded according to the National Cancer Institute Common Terminology Criteria for Adverse Events, version 4.0. Response was assessed at weeks 8 and 12 and subsequently every 12 weeks according to Response Evaluation Criteria in Solid Tumors (RECIST), version 1.1 based on investigator assessment.

Patient samples

Eighty-two patients were enrolled on the study. These included 34 patients with melanoma (68% male), 27 patients with NSCLC (44% male), and 21 patients with bladder cancer (71% male). Leukaphereses, blood, and serum samples were obtained from study participants throughout treatment. Leukaphereses were obtained at pre-treatment, pre-vaccine (week 10-12) and post-vaccine (week 20). Blood and plasma samples were obtained at weeks 6, 14, 16 and 24. Patient PBMCs were isolated within 4h after blood collection using Ficoll-paque (GE Healthcare) density-gradient centrifugation and cryopreserved in Recovery Cell Culture Freezing Medium (Invitrogen). PBMCs were stored in vapor-phase liquid nitrogen and plasma samples were stored at $-80^{\circ}C$ until time of analysis.

Tumor samples (surgical and core-needle biopsies) were obtained at pre-treatment, pre-vaccine (week 10-12) and post-vaccine (week 24). Samples were fixed in 10% neutral-buffered formalin for at least 18 and no more than 30h and then processed and embedded in paraffin by traditional vacuum infiltration tissue processing techniques. Pre-treatment biopsies were used for generation of NEO-PV-01 and were advanced for DNA and RNA sequencing only if 5 cores or $100mm^3$ were available and if pathology review indicated a tumor cellularity $\geq$ 30%. If none of the core biopsies met the minimum 30% tumor cellularity, enrichment by macrodissection may have been performed. In several instances, archival biopsies were permitted, if they had been obtained within 180 days of patient consent and if there had been no intercurrent therapy.

METHOD DETAILS

Generation of NEO-PV-01

Whole exome sequencing

WES (library protocol: ACE(TM) Cancer Research Exome, Personalis, Menlo Park, CA) and RNA-Seq (library protocol: ACE(TM) Cancer Research Transcriptome, Personalis, Menlo Park, CA) libraries were sequenced using Illumina HiSeq in a CLIA/CAP accredited laboratory (Personalis, Menlo Park, CA). WES was conducted on a tumor sample and a normal blood sample per patient (depths: 158-347 reads and 65-289 reads, respectively); RNA-Seq was conducted on tumor samples only (depth: 94-547 reads).

The HLA-A and HLA-B genotype of each patient was determined by amplifying informative exons by polymerase chain reaction (PCR) using locus-specific primers. Dye-terminator sequencing fragments from the PCR fragments were analyzed on a capillary sequencer to determine nucleotide sequences for each haplotype (BloodCenter of Wisconsin, Milwaukee, WI).

Alignment and mutation calling

All computational analysis steps were conducted using an automated analysis pipeline hosted on a cloud computing platform (Seven Bridges Genomics, Charlestown, MA).

Tumor and germline WES and tumor RNA-Seq FASTQs were aligned to the human genome (Gencode V19) using the BWA-MEM (version 0.7.13) (Li and Durbin, 2009) and STAR (version 2.5.1.b), respectively. All alignments were post-processed with the GATK 3.5 workflow (McKenna et al., 2010) including GATK Indel Realigner, GATK Base Recalibrator, and Picard Mark Duplicates (version 1.140). ConTest (Cibulskis et al., 2011) was used to confirm that all three samples originated from the same individual.

Somatic variants were called on the basis of tumor and normal WES using an ensemble of seven different mutation calling algorithms: VarDict (version 1.4.6) (Lai et al., 2016), Strelka (version 1.0.15) (Saunders et al., 2012), VarScan2 (version 2.3.9) (Koboldt et al., 2012), Mutect2 (from the GATK version 3.5 bundle) (Cibulskis et al., 2013), Atlas Indel2 (version 1.4.3) (Challis et al., 2012), Seurat (version 2.6) (Christoforides et al., 2013), and Platypus (version 0.8.1) (Rimmer et al., 2014). The three sequencing datasets were then realigned using HaplotypeCaller (from the GATK version 3.5 bundle), specifying the candidate mutations (union of the seven call sets) as known variants. Finally, the variants were filtered according the following features: the level of read support in the tumor WES data, the presence of variant reads in the normal WES data, read orientation bias, adequacy of coverage in the normal WES sample, the presence of neighboring (+/−30nt) variants (somatic or germline), and read quality bias observed in mutation-supporting reads.

RNA-Seq expression levels of all genes and transcripts were quantified in transcripts per million (TPM) using RSEM (version 1.2.31) (Li and Dewey, 2011). The overall expression of each somatic variant was calculated as the product of the RSEM-derived transcript expression (summing across all overlapping protein-coding transcripts) and the fraction of RNA-Seq reads supporting the variant. Variants with zero supporting RNA reads were still considered as valid mutations (and counted toward tumor mutation burden) but were not considered for inclusion in vaccine. RNA-Seq was additionally processed using STAR-Fusion (version 2.5.1.b) (Haas et al., 2017) to identify transcript fusions (requiring both junction support and spanning read pairs).

In the event that an adequate RNA library could not be prepared (patients: B9 and M17), fusion calling was skipped and reference expression was obtained from TCGA samples with high tumor purity (as assessed by Absolute; five samples per tumor type) (Carter et al., 2012). Since these patients lacked RNA-Seq as a filter against false positive mutation calls, their somatic variants were required to have a higher level of read support in the tumor WES and to have been identified by more than one mutation caller.

Vaccine peptide selection

Patients with at least 50 non-synonymous point mutations and/or gene fusions were advanced to the vaccine design step. The vaccine peptides, also referred to as immunizing (IM) peptides, were identified by selecting 6 peptides on the basis of HLA-I presentation scores (also referred to as epitope quality scores, see below), 2 peptides based on high expression, and 2 peptides based on highly expressed frameshifts, iteratively until the full roster of 30 peptides was completed. HLA-I epitopes were required to have a NetMHCpan (version 3.0) percent rank lower than 2%, and the latter two epitope classes were required to have expression levels > 10 TPM and > 5 TPM, respectively (if none were available, the slots were ceded to HLA-I selections). Generally, each mutation was targeted by only one vaccine peptide and excluded from subsequent selections unless the span of novel sequence generated could not be covered by a single peptide (as can happen with frameshifts) or if the likelihood of manufacturing success was questionable for the first peptide per known synthesis constraints. The trade-off between synthesis constraints and immune-related scoring further dictated the relative length of the vaccine peptides (allowable range: 14-35 amino acids) and whether they were centered or shifted with respect to the site of mutation.

HLA-I presentation scores were determined based on a logistic regression that considered binding affinity (NetMHCpan-3.0 percent rank) (Nielsen and Andreatta, 2016), allele-specific expression, and proteasomal cleavage potential (using a previously described prediction approach); the weights of the logistic regression were optimized according to mass spectrometry data as previously described (Abelin et al., 2017). The score of a candidate vaccine peptide was determined by summing all the relevant peptide-allele combinations (epitopes lengths 8-11; HLA-A and HLA-B alleles only).

Secondary characteristics were used to up-weight and down-weight candidate epitopes but were purposely tuned to have less importance than the above-mentioned factors. Thus, all other parameters being equal, the selection algorithm favored more clonal epitopes (higher mutant allele fraction) over sub-clonal epitopes, frameshifts over point mutations, oncogenes over passenger genes, and peptides with good manufacturing scores over those with poor predicted manufacturability. Our scoring system did not consider the relative binding scores of wild-type peptides or similarity to known pathogen sequences (Łuksza et al., 2017) .

GMP peptide manufacturing

The GMP grade peptides of NEO-PV-01 were synthesized using solid-phase peptide synthesis (SPPS) on automated parallel peptide synthesizers. 9-fluorenylmethyloxycarbonyl (Fmoc) chemistry was employed. After the assembly of the peptide chains, the peptides were removed from the resins using cleavage cocktails containing trifluoroacetic acid and scavengers. The peptides were precipitated and washed with ether. After drying, the crude peptides were purified on automated preparative high-performance liquid chromatography (prep HPLC) systems with ultraviolet (UV) and mass spectrometry (MS) detectors. The prep HPLC fractions were analyzed using ultra-performance liquid chromatography (UPLC)-UV/MS systems to determine molecular weights (MW) and purities. The fractions containing the target peptides and desired purities were lyophilized to solid powders with the final purities equal to or higher than 95%. Up to 20 peptides per vaccine were formulated in a buffered aqueous solution containing 4% DMSO in isotonic dextrose and mixed into up to four pools, each containing up to five peptides. The pooled peptide solutions were filtered through 0.22 μm filters for sterilization. The vaccines were analyzed for identity (molecular weights based on UPLC-UV/MS analysis), sterility,

endotoxin, and strength before their releases from the GMP manufacturing site. The amino- and carboxyl-termini of the peptides are free amines and carboxylic acids respectively, without structural modifications.

Peptide synthesis for immunological assays

The peptides for *in vitro* immune response studies were synthesized using SPPS on computer-controlled high-throughput peptide synthesizers. The peptides were assembled on resins by employing Fmoc-chemistry. The chemical cleavages of peptides from the resins were performed by using TFA solution containing scavengers followed by peptide precipitation and washes with diethyl ether. The assay peptides (ASP) were purified on automated prep HPLC systems equipped with UV and MS detectors. The prep HPLC fractions of each peptide that met the molecular weight (MW) and purity criteria based on UPLC-UV/MS analysis were pooled and dried using either parallel centrifugal evaporators or lyophilizers. The epitope peptides (EPT) were resuspended in acetonitrile and water and dried on a lyophilizer after diethyl ether washes and analyzed for required purity and MW by using UPLC-UV/MS. Assay peptides (ASP) were 13-15 amino acids and overlapped by at least 9 amino acids to cover the immunizing peptide (IM) sequence or were 8-11 amino acids and predicted to bind class I (Ott et al., 2017). All assay peptide sequences are provided in Table S8.

Detection of neoantigen-specific immune responses

For *ex vivo* assays, patient PBMCs were rested overnight at 2×10^6 cells/mL in X-Vivo media (Lonza) supplemented with 1% penicillin/streptomycin (GIBCO). For neoantigen pre-exposure assays, patient PBMCs were rested overnight and cultured with individual peptides (2 μM) or pooled peptides (2 μM per peptide) for 5 days at a density of $5x10^6$ cells/ml in a 24-well plate. On day 3 of culture, half the well volume was replaced with fresh media. All immunizing peptides were tested in both the *ex vivo* as well as in the 5-day stimulation with the neoantigen peptide assay formats. Immunizing peptides are referred to as IM followed by the peptide number.

IFN−γ ELISpot assay

IFN-γ ELISpot assays were performed using 96-well MultiScreen Filter Plates (Millipore) and the Ready-Set-Go! Human IFN-γ ELISpot Kit (Invitrogen) according to manufacturer's instructions. Plates were coated overnight at 4°C with anti-IFNγ Capture Antibody diluted in 1X Coating Buffer, washed with 1X Coating Buffer and blocked with X-Vivo media (Lonza) containing 1% penicillin/streptomycin (GIBCO) for 1h. For *ex vivo* ELISpots, PBMCs were plated in triplicate with 1×10^6 cells per well. For cells that were pre-exposed to peptide, cells were washed and plated in triplicate with 1×10^5 cells per well. Peptides were added to ELISpot wells at 2 μM per peptide. Each plate included a healthy donor positive and negative control with the CEF viral peptide pool (JPT) and Cell Stimulation Cocktail (Life Technologies) to confirm reagent performance. Plates were incubated overnight at 37°C. Plates were washed 3 times using PBS with 0.05% Tween-20 and detection antibody diluted in 1X ELISpot diluent was added to wells for 2h. After washing 3 times with PBS with 0.05% Tween-20, Avidin-HRP was diluted in 1X ELISpot diluent and added to wells for 45 min. Plates were washed with both PBS with Tween-20 and PBS 3 times. AEC substrate-chromogen (BD Biosciences) was then added for 20 min. Plates were rinsed with deionized water 3 times and allowed to dry at room temperature overnight. Spots were imaged and enumerated using an Immunospot analyzer (Cellular Technology Limited). Responses were characterized as positive if spot-forming cell count detected was at least 10 spots over the DMSO control and +3 standard deviations and confirmed in repeat experiments.

Characterization of $CD4^+$/ $CD8^+$ T cell responses

$CD3^+$ T cells were isolated from patient PBMCs by negative selection using the Pan T cell isolation kit (Miltenyi). Both the $CD3^+$ and $CD3^-$ populations were collected, washed, and counted after isolation. The CD3- population was used as APCs (antigen presenting cells) for this assay. The $CD3^+$ population then underwent $CD4^+$ positive isolation using $CD4^+$ microbeads (Miltenyi). Both the $CD4^+$ (positive-selection) and $CD8^+$ (negative-selection) T cells were collected, washed, and counted. A co-culture containing APCs and either $CD4^+$ or $CD8^+$ cells at a ratio of 3:1, 2:1, or 1:1 were plated in a 96-well flat bottom polystyrene plate for 24-48h. Peptide was added directly to wells, in triplicate, at 2 μM per peptide. If the T cells were pre-exposed to neoantigen peptide for 5-6 days, $CD3^-$ APCs were isolated from fresh patient PBMCs using CD3 microbeads (Miltenyi). Supernatants were collected at the end of the coculture and frozen at −80°C until use.

The Meso Scale Discovery (MSD) U-Plex system was used to detect 10 distinct analytes from the coculture supernatants. The analytes measured were: IL-1β, IL-2, IL-6, IL-9, IL-13, IL-15, IL-17a, IFN-γ, and TNF-α. MSD 10-plex plates were coated with the linker-antibody solution for 1h with shaking at room temperature. The plates were then washed 3 times with PBS with 0.05% Tween-20 on a BioTek plate washer. Supernatant and standards were diluted 1:2 and added to the plate for 1h with shaking at room temperature. Plates were washed again with PBS with 0.05% Tween-20 before the addition of the detection antibody solution for 1h. Plates were washed with PBS with 0.05% Tween-20 and 2X Read Buffer (MSD) was added to the plates for detection on the MSD SECTOR S 600 instrument. Concentration in pg/mL was calculated by the MSD Discovery Workbench software by comparing luminescent signal of the patient samples against the known standard curve. $CD4^+$ and $CD8^+$ positive responses were determined separately based on the corresponding DMSO controls. A positive signal was determined by an IFN-γ signal 1.5-fold higher than the DMSO control.

MHC class I tetramer production and staining

Recombinant pMHC-I monomers with UV cleavable conditional ligands were prepared for analysis of vaccine-induced neoantigen-specific CD8+ T cells. The gene sequences of the human class I HLA heavy chains were identified from the IPD-IMGT/HLA webpage (https://www.ebi.ac.uk/ipd/imgt/hla) and codon-optimized for expression in *E. coli* using commercially available algorithms (Genewiz). The extracellular domain of class I heavy chain (amino acid residues 1-276) was fused to a C-terminal GSGGSGGSAGG linker and a GLNDIFEAQKIEWH biotinylation tag and cloned via the NdeI and BamHI restriction sites into the bacterial expression vector pET22b (Millipore Sigma). The human β2 m sequence (amino acid residues 1-99) was cloned into pET22b via the NdeI and BamHI restriction sites.

The HLA heavy chains were expressed in BL21 (DE3) cells (NEB) grown in LB media at 37°C to an OD600 of 0.8 followed by induction with 1 mM Isopropyl-β-D-1-thiogalactopyranoside for 4h. The human β2 m protein was expressed in BL21 (DE3) cells grown in Studier ZYM-5052 auto-induction medium at 37°C to an OD600 of 0.8 followed by a temperature shift to 20°C for overnight growth. Both proteins accumulate in inclusion bodies which were isolated from the *E. coli* cells using a previously described protocol and solubilized in 100 mM Tris-HCl, pH8.0, 8M Urea for subsequent refolding (Rodenko et al., 2006). UV conditional ligand (CL) peptide-loaded pMHC-I monomers were refolded by mixing 3 μM class I heavy chain with 6 μM β2 m and 10 μM CL peptide in refolding buffer (100 mM Tris-HCl pH8, 400 mM L-arginine, 2 mM EDTA, 5 mM reduced glutathione, 0.5 mM oxidized glutathione, 15% glycerol, 3 mM PMSF and 1X CompleteTM EDTA free-protease Inhibitor Cocktail (Roche)) and incubated at 4°C for 5 days (Garboczi et al., 1992; Rodenko et al., 2006; Toebes et al., 2006). The refolded trimetric HLA complex was subsequently buffer exchanged on a SARTOFLOW-R (Sartorius) crossflow system against 20 mM Tris-HCl pH8, 25 mM NaCl, 15% glycerol and loaded on a HiTrap Q HP anion exchange chromatography column followed by elution with a continuous salt gradient elution to 500 mM NaCl on a ÄKTAPurifier system (GE Healthcare). Fractions containing refolded pMHC-I monomers were identified, pooled and concentrated to 60 μM in 500 mM Bicine, pH 8.3. 100 mM ATP, 100 mM MgOAc, 1 mM biotin for biotinylation for 3h at 30°C with 1 μM recombinant BirA (Abelin et al., 2019). The reaction mixture was then concentrated to 5 mL and loaded on a Yarra S2000 (Phenomenex) column equilibrated in 1xPBS+16% (v/v) glycerol to separate the biotinylated pMHC-I monomers from other components of the biotinylation reaction by size exclusion chromatography on a ÄKTAPurifier system (GE Healthcare). The pMHC-I monomer product was flash-frozen in liquid nitrogen at a concentration of 2 mg/mL and stored at −80°C until further use.

Tetramer preparation for PBMC staining

Peptide MHC multimers were generated by irradiating UV-cleavable monomers (0.1mg/mL) in the presence of EPT (9-12 amino acids) peptides (10mM in DMSO) at a 1:50 ratio under UV light (365 nm) at 4°C for 1h, followed by a 1h incubation at 37°C. Exchanged monomers were centrifuged at 3600RPM for 10 min. The exchanged monomer supernatant was incubated with fluorochrome conjugated streptavidin antibodies on ice for 30 min in the dark. Excess biotin (1:20 dilution) was added after incubation and exchanged fluorochrome-conjugated multimers were stored at 4°C until staining.

Patient PBMCs were treated with benzonase and dasatinib, both at a 1:1000 dilution, and were incubated for 30 min at 37°C. Samples were centrifuged at 1500RPM for 5 min, washed once in FACS buffer containing dasatinib, and resuspended with the pooled multimer mixture at a final staining volume of 50 μL per sample with FACS buffer containing dasatinib. Samples were incubated with multimers at 37°C for 15 min, and subsequently stained with the appropriate surface antibodies for 30 min on ice. After incubation, samples were washed once with FACS buffer containing dasatinib and resuspended in 200 μL FACS buffer containing dasatinib. Samples were acquired on a BD LSR Fortessa instrument.

CD107a mobilization assay

For *ex vivo* detection, patient PBMCs were recalled with 2 μM peptide or DMSO for 6 or 24h. For patient PBMCs pre-exposed to neoantigen peptide, $CD3^-$ APCs were isolated from fresh PBMCs using CD3 microbeads (Miltenyi) and co-cultured with $CD3^+$ T cells at a T cell:APC ratio of 2:1 and recalled with 2 μM peptide or DMSO for 6 or 24h. Anti-CD107a antibody was added 6h prior to the end of co-culture. GolgiStop/Plug (BD Biosciences) were added 4h prior to the end of co-culture. Subsequently, cells were stained with cell surface antibodies at 4°C for 30 min, followed by fixation/permeabilization with Fixation and Permeabilization Solution (BD Biosciences), and subsequently stained with antibodies against intracellular proteins at 4°C for 30 min. Cells were stored in FACS buffer at 4°C until acquisition on a BD LSR Fortessa instrument.

Phenotyping and ICS of neoantigen-specific T cells

For intracellular cytokine staining (ICS), patient PBMCs were stimulated with 2 μM peptide or DMSO for 6 or 24h. GolgiStop/Plug (BD Biosciences) were added 4-5h prior to end of recall period with peptide. For phenotyping, patient PBMCs were treated with dasatinib at a 1:1000 dilution in X-Vivo media (Lonza) at 37°C for 30-60 min followed by staining with tetramers (if applicable) at 4°C for 30 min. For both assays, patient PBMCs were treated with benzonase (Millipore) at a 1:1000 dilution in X-Vivo media (Lonza) at 37°C for 30-60 min, followed by staining of surface antibodies. Cells were fixed at 20°C for 30 min using the Foxp3/Transcription Factor Staining Buffer Set (eBioscience) for phenotyping, and with the Intracellular Fixation and Permeabilization Buffer Set (eBioscience) for ICS, and subsequently stained for intracellular proteins at 4°C for 30 min. Cells were stored in FACS buffer at 4°C until acquisition on a BD LSR Fortessa instrument.

Phenotypic analysis of peripheral samples

Patient PBMCs were treated with benzonase (Millipore) at a 1:1000 dilution in X-Vivo media (Lonza) at 37°C for 30 min. A total of 2 × 10^6 cells per sample were plated for flow staining and washed once with FACS buffer (PBS + 0.5% BSA). Cells were then incubated with cell surface antibodies for 30 min on ice, followed by a wash with FACS buffer. Cells were fixed and permeabilized for intracellular staining using either the BD cyofix/cytoperm kit (BD Biosciences) or Foxp3/Transcription Factor Staining Buffer Set (eBioscience) according to the manufacturer's instructions for 20 min on ice. Cells were then incubated with intracellular antibodies in the corresponding permeabilization wash buffer for 30 min on ice, washed with the appropriate permeabilization wash buffer and followed by a final wash with FACS buffer. Cells were stored in FACS buffer at 4°C until acquisition on a BD LSR Fortessa instrument.

RNA extraction from FFPE tumors and PBMCs

For FFPE tumor blocks, 2-4 scrolls of 20 μM thickness were deparaffinized using heptane and RNA was extracted using the AllPrep DNA/RNA FFPE kit according to the manufacturers' instructions (QIAGEN). For PBMC samples, $CD3^+$ T cells were isolated using the Pan T cell Isolation Kit (Miltenyi) and subjected to RNA extraction using RNeasy Plus Mini or Micro Kit according to manufacturer's instructions (QIAGEN). RNA was quantified using the Qubit RNA HS Assay Kit (ThermoFisher) according to manufacturers' instruction. Quality and size distribution of extracted RNA was determined on an Agilent Bioanalyzer 2100 using either the RNA 6000 Nano Kit or RNA 6000 Pico Kit (Agilent).

TCR sequencing

Bulk TCR sequencing was performed on RNA samples extracted from patient FFPE tumor blocks and $CD3^+$ T cell enriched PBMCs. Up to 1 ug of RNA was submitted to iRepertoire for targeted TCR sequencing (Wang et al., 2010) or processed according to iRepertoire protocol and sequenced using Illumina sequencers at a depth of ~1 million reads per sample. BCL files were converted to FASTQ format. The first three bases of each read were trimmed, and the samples were then demultiplexed using either through the Illumina built-in software or the fastq-multx function from the ea-utils package (Aronesty, 2011). TCR repertoire data were generated from raw demultiplexed data using MiXCR, version 3.0.12, (Bolotin et al., 2015). Analysis of TCR repertoire characteristics and features was performed in the R environment for statistical computing. Unless specifically stated, analyses were performed on the amino acid (AA) TCRbeta-CDR3 clonotypes, aggregating counts from various nucleotide CDR3 sequences encoding the same AA CDR3. Non-functional (out-of-frame or containing stop codons) CDR3 were excluded.

The unbiased gini coefficient, indicating the inequality in the AA CDR3 frequency distribution, was calculated using the "Gini" function from the DescTools package (Signorell et al., 2016), using the counts of all detected functional AA CDR3 clonotypes in each sample. The unbiased gini coefficient ranges from "0" (complete equality) to "1" (complete inequality).

The DE50 coefficient, a diversity and clonality index representing the minimal number of clones to cover half of the overall frequency space, was calculated by ranking the clones based on their AA CDR3 frequency from high to low. The rank of the clone was then obtained at which the cumulative frequency reaches 50% of the total sum of repertoire frequencies with low numbers indicating high clonality. The DE50 is the obtained rank divided by the maximal rank of the sample (the number of unique AA CDR3 clonotypes).

For single-cell TCR sequencing (scTCRseq), patient PBMCs were sorted in 96-well plates either based on tetramer staining or staining with T cell activation markers (CD69, CD107a, CD25, PD-1) after neoantigen peptide exposure for 5-6 days and recall for 6-24h. Final sort gates for neoantigen-reactive subpopulations were determined based on control tetramer staining or control cocultures with DMSO. Plates were submitted to iRepertoire for scTCRseq (iPair-TCR). Paired sequencing information was used to determine clonal composition of sorted cell populations and candidate alpha/beta chain pairs were tested for neoantigen-reactivity after lentivirus-based T cell transductions (Banu et al., 2014)

Cloning of neoantigen-specific TCRs

Second generation lentivirus vectors were generated on 293FT producer cell lines using shuttle plasmids (GenScript) containing TCR beta and alpha chains under the control of a SFFV promoter and separated by a furin cleavage site and a P2A ribosomal skip sequence. Human TCR variable regions were fused to cysteine-modified mouse constant regions for both chains resulting in recombinant mTCR (Cohen et al., 2006; Kuball et al., 2007). Neoantigen-reactivity of mTCR Jurkat cells was determined by IL-2 secretion measured by electrochemiluminescence (MSD) in 24h co-culture assays of mTCR transduced Jurkat cells with neoantigen peptide and allele matched antigen presenting cell lines or $CD3^+$ T cell depleted autologous patient PBMCs. Cytotoxicity of recombinant mTCR transduced PBMCs was assessed based on CD107a surface staining of effector cells and activated caspase-3 staining of target cells.

Cytotoxicity assay

A375 target cells (ATCC) that were HLA-matched to the patient peptide of interest were harvested and plated in DMEM, high glucose, GlutaMAX Supplement, pyruvate (Thermo Fisher) supplemented with 10% FBS (Corning) at a density of 100,000 cells/well in a 96-well plate. The following day, the A375 cells were loaded with EPT length peptides (either containing the mutation or wild-type) by replacing the media in the wells with fresh AIM V Medium (GIBCO) containing peptide at a 2 μM final concentration. Patient PBMCs from the pre-treatment time point were enriched for $CD3^+$ T cells using the Pan T Cell Isolation Kit (Miltenyi). Isolated $CD3^+$ T cells

were transduced with neoantigen-specific TCRs and cocultured with target A375 cells at varying effector:target ratios for a period of 6 or 24h.

Gene expression

Targeted gene expression analysis on total RNA extracted from FFPE blocks was performed using the NanoString nCounter platform (NanoString Technologies). A custom code set consisting of 800 genes, including markers for immune cell populations, cytolytic markers, immune activation and suppression, and the tumor microenvironment, was used. For each sample, either 50ng or 100ng of total RNA was hybridized with the custom gene expression code set for 16h at 65°C according to the manufacturer's protocol. Hybridized samples were run on the NanoString nCounter SPRINT Profiler instrument (NanoString Technologies). Raw data was normalized to the 30 housekeeping genes included in the custom code set using the nSolver software (version 3.0). Modified PanCancer IO360 gene signature scores were calculated and provided by NanoString Technologies. Additional gene signature scores were calculated in house using normalized gene expression.

APOE Genotyping

To assess the APOE genotype from patients, whole exome sequencing data (aligned to hg19) was queried for allele frequencies using pysam (v0.15.2)(Li et al., 2009) at genomic locations chr19:45411941 (site A) and chr19:45412079 (site B) as determined in Atherosclerosis Risk in Communities (ARIC) study (Blair et al., 2005). APOE E4 genotype was assigned if site A and B were both homozygous for cytosine.

Immunohistochemistry

For each patient FFPE tumor block, histological and immunohistochemical analysis was done at Mosaic Laboratories (Lake Forest, CA). H&E analysis was performed according to Mosaic Laboratories' optimized protocols and reviewed for cellular quality, morphology, and presence of tumor by an independent pathologist. Immunohistochemical analysis for PD-L1 (DAKO kit, MOS504-APD) was performed according to Mosaic Laboratories' optimized protocols. Staining was evaluated using ImageScope software and standard pathology review. PD-L1 staining was evaluated using scoring criteria provided by Bristol-Myers Squibb.

Immunohistochemistry for CD3 was performed on 5μm FFPE tumor sections. Slides were baked at 60°C overnight, dewaxed and rehydrated. Antigen retrieval was performed using a microwave (MWT) with antigen retrieval buffer (citric acid based, pH 6.0, Vector Labs) heated to 90°C for 15min. After cooling to room temperature (RT), slides were washed with TBST/0.5% Tween and blocked for 10min with Akoya blocking buffer (Akoya Biosciences). Primary antibody CD3 (Biocare Medical, clone LN10, 1:100) was incubated at RT for 30min. Slides were washed and incubated with HRP-conjugated secondary antibody diluted 1:1 in TBS for 30min (Vector Labs). CD3 was visualized with ImmPACT Vector Red chromogenic staining.

Multiplex IHC staining protocol

Manual multiplex immunofluorescence (mIF) staining was performed on 5μm FFPE tumor sections using the TSA Plus Fluorescence kit (Akoya Biosciences). Slides were baked at 60°C overnight, dewaxed and rehydrated. Antigen retrieval was performed using a microwave (MWT) with antigen retrieval buffer (citric acid based, pH 6.0, Vector Labs) heated to 90°C for 15min. After cooling to room temperature (RT), slides were washed with TBST/0.5% Tween and incubated with 3% H_2O_2 for 15min. Next, slides were blocked with 2% BSA, 5% NHS in TBST for 1h. Primary antibody TCF7 (Cell Signal Technology, clone C6D9, 1:50) was incubated at RT for 1h. Slides were washed and incubated with HRP-conjugated secondary antibody diluted 1:1 in TBS for 30min (Vector Labs). TCF7 was visualized with TSA Cy5 (1:50) for 10 min.

Multiplex staining was performed by repeating staining cycles with MWT heating between each step to remove the antibody complex. Successive antibodies include: CD8 (Biocare Medical, clone SP16, 1:100, TSA plus Cy3) and S100 (Biocare Medical, clone 15E2E2&4C4.9, 1:100, TSA Fluorescein) each incubated for 30min. Secondary HRP antibodies were diluted 1:1 with TBS and incubated for 30min (Vector Labs). Nuclei were stained with DAPI 1:3000 for 10min (Fisher Scientific), washed and mounted with Prolong gold (Fisher Scientific). Human tonsil FFPE tissues were used with and without primary antibodies to serve as positive and negative (autofluorescence) controls.

QUANTIFICATION AND STATISTICAL ANALYSIS

Multispectral analysis

The multiplex slides were scanned with a Vectra 3.0 microscope system (Perkin Elmer). Whole slide scans were performed using the 10x objective lens. Up to ten individual fields were selected in the Phenochart program (Phenochart 1.0.9, Perkin Elmer) for higher resolution scanning at 20x (669x500 μm). Multispectral images were unmixed and analyzed using inForm software (inForm 2.4.2, Perkin Elmer) and analyzed with tissue component segmentation based on tumor cell staining: tumor = S100+ regions and stroma = S100- regions. Individual cells (defined by DAPI positive nuclei) were then phenotyped to characterize various cell populations. Density of cells in each ROI was calculated by combining the cell counts from all images and normalizing by the total area (cells/mm^2).

Statistical analysis

Anti-tumor activity was assessed for objective response rate (ORR), duration of response (DOR), progression free survival (PFS) and overall survival (OS). ORR is defined as the proportion of patients who achieve CR or PR based on RECIST v1.1. DOR is defined as the date of the first documented confirmed response to the date of the first documented PD or death. PFS is defined as the time from the date of first dosing to the date of first documented PD or death. OS is defined from the date of enrollment to death. Statistical efficacy analyses were performed separately for each indication for both the ITT set defined as receiving at least one dose of nivolumab and the safety set defined as receiving at least one dose of vaccine. The Kaplan–Meier method was used to estimate PFS and OS. For PFS, patients who did not have PFS event on study or who were lost to follow-up were censored at the time of last tumor assessment. For OS, patients who were alive or who were lost to follow-up were censored at the last record on database.

All other analyses were performed in either the R language and environment for statistical computing (version 3.5.1) or GraphPad Prism (version 7.01). Likewise, all figures were created using an R script on the ''ggplot2'' package (Wickham, 2016) or GraphPad Prism. Unless otherwise specified, p values were derived from a two-tailed Student's t test.

ADDITIONAL RESOURCES

All data presented in this manuscript is from the multicenter phase I clinical trial NCT02897765. https://clinicaltrials.gov/

Supplemental Figures

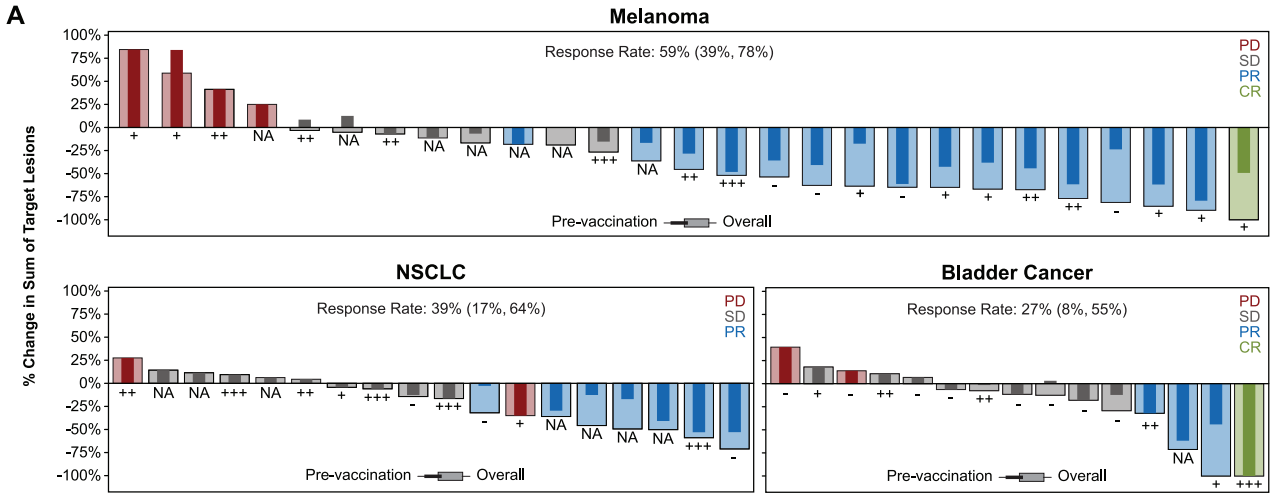

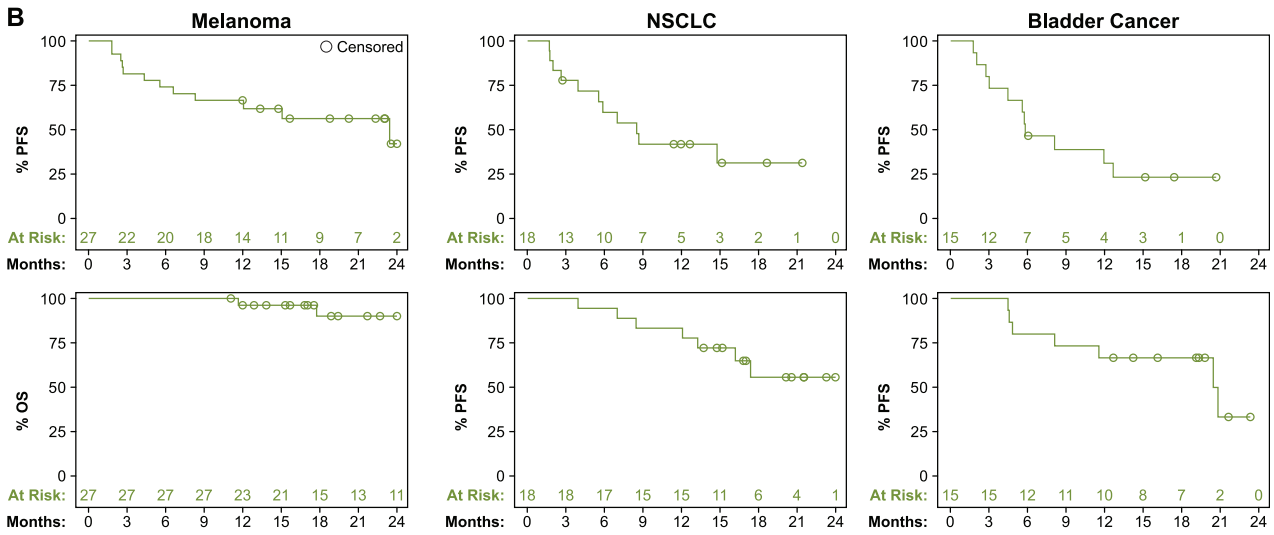

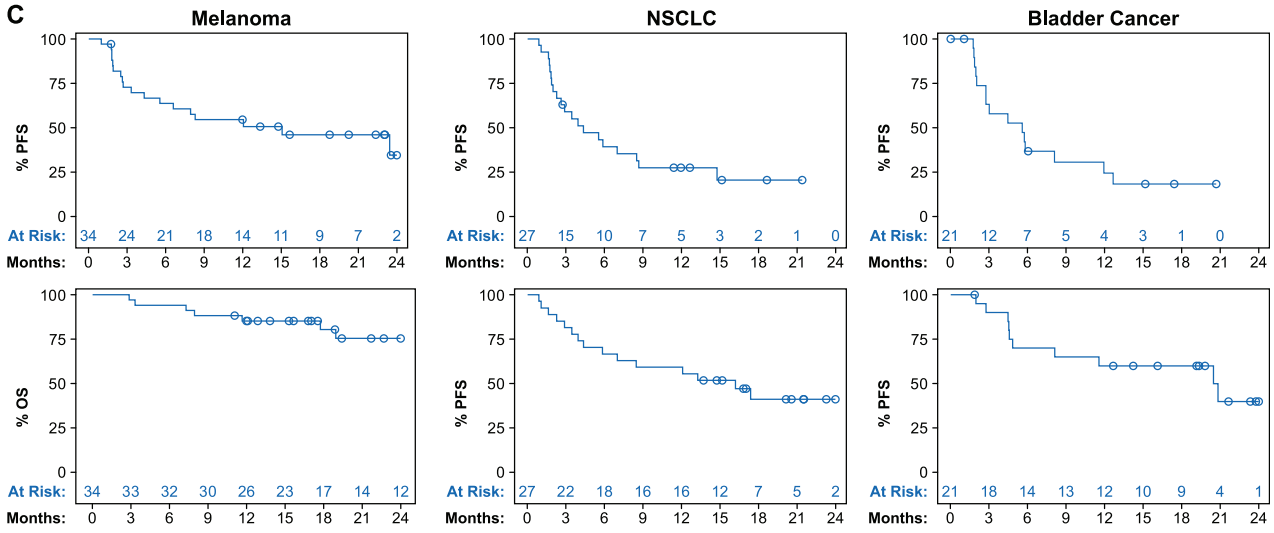

(legend on next page)

Figure S1. Radiographic Responses with Pre-treatment Tumor PD-L1 Levels in Vaccinated Patients and OS/PFS by Tumor Type; Additional Data Related to Figure 2

(A): Radiographic responses with pre-treatment PD-L1 levels in tumors of patients who received at least one dose of NEO-PV-01. PD-L1 levels are indicated below the bars in the waterfall plots for the three tumor cohorts. Scoring was based on percent PD-L1 on tumor cells as follows: < 1% is indicated as -, ≥ 1% as +, ≥ 5% as ++ and ≥ 50% as +++. NA: data not available. (B and C): Kaplan-Meier estimates of PFS (top panel) and OS (bottom panel) for all three tumor types in patients who received > = 1 dose of vaccine (B) and in all patients who received at least one dose of nivolumab (ITT, C).

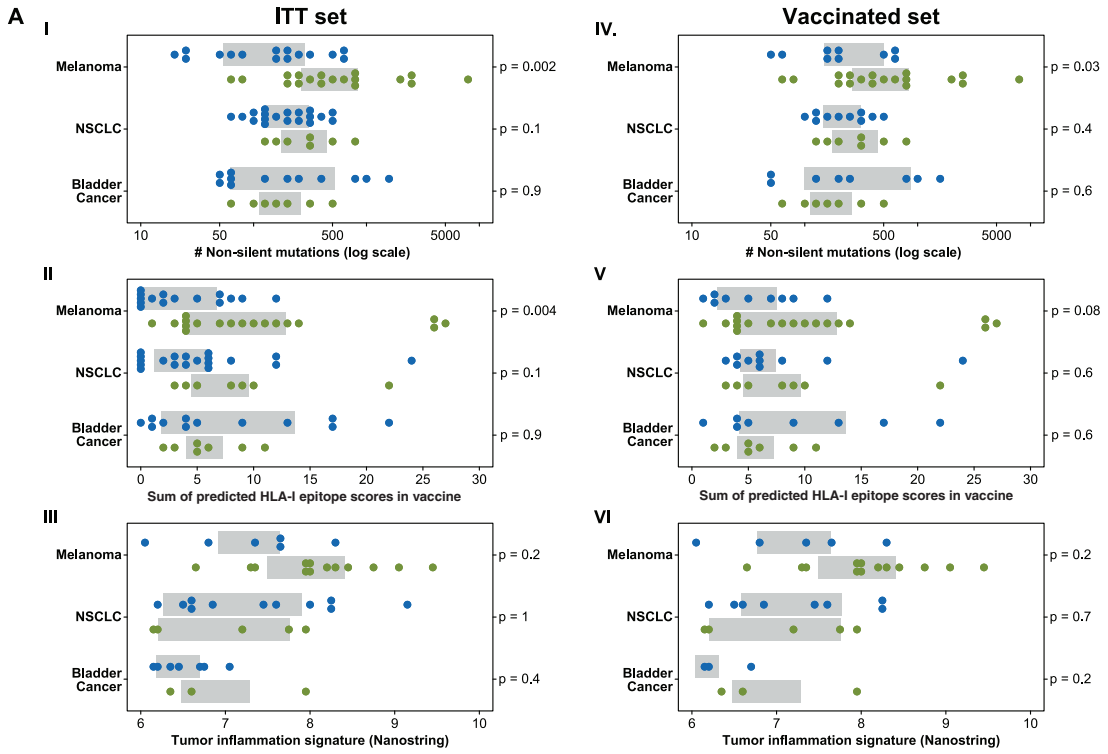

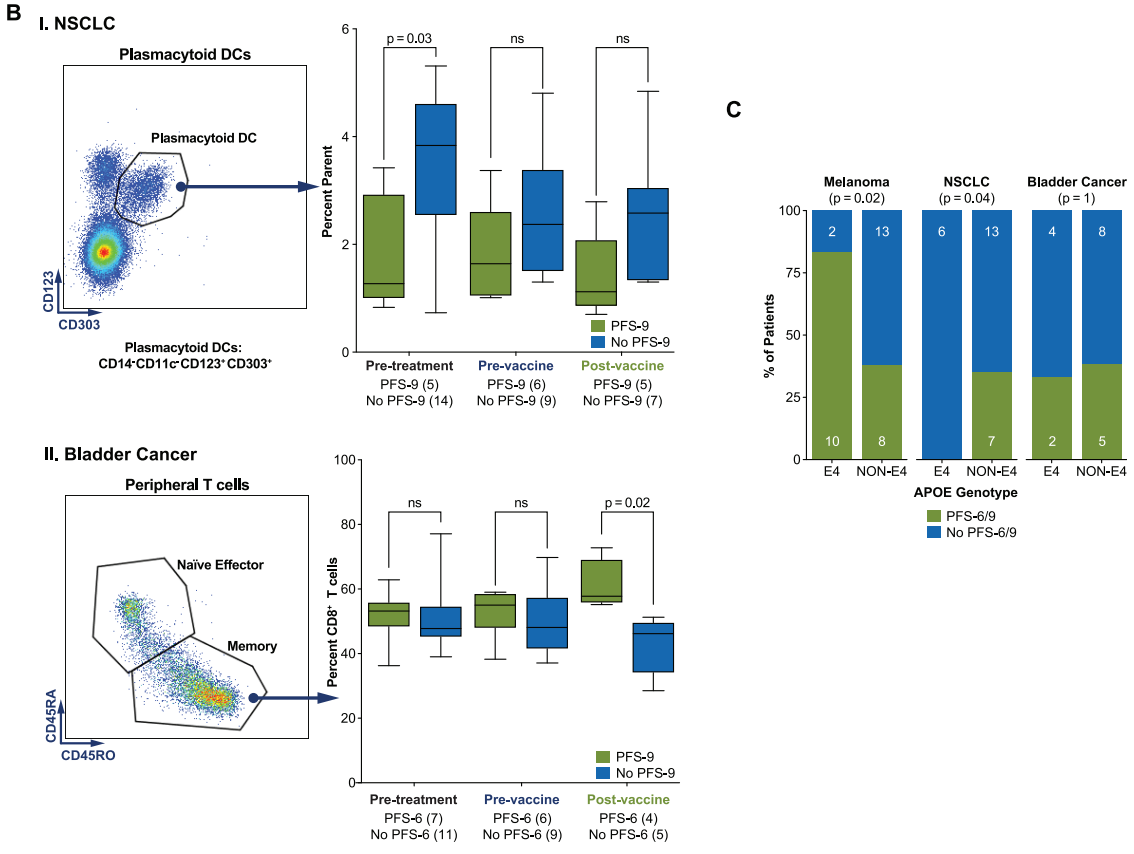

(legend on next page)

Figure S2. Distinct Molecular and Immune Features Are Associated with PFS across the 3 Tumor Cohorts; Additional Data Related to Figure 3

A: Tumor mutation burden, epitope quality score, and gene expression with PFS; Molecular correlations of PFS-9 in the melanoma and NSCLC and PFS-6 in the bladder cancer cohorts. PFS-9/6 is defined as lack of disease progression at nine months post-initiation of anti-PD-1 therapy for the melanoma and NSCLC cohorts, respectively, and lack of disease progression at six months for the bladder cancer cohort. Panels i, ii, and iii include patients in the ITT set and panels iv, v and vi include patients who received at least one dose of NEO-PV-01 (vaccinated set). I and IV) Each dot depicts tumor mutation burden (total number of non-silent mutations) of individual melanoma patients with PFS-9 (green) and without PFS-9 (blue). Gray boxes indicate interquartile ranges; p values are calculated using Wilcoxon rank-sum test. II and V) Analogous plots for the HLA class I epitope quality scores of vaccinating epitopes for melanoma patients. The epitope quality score of each candidate epitope falls on a 0-1 scale with higher scores corresponding to increased likelihood of presentation. Values are summed across the potential HLA-I epitopes for all vaccinating peptides per patient. III and VI) Analogous plots for T cell inflammation score (TIS) at the pre-treatment time point as assessed by gene expression analysis on the NanoString^{TM} platform. TIS score was calculated as previously described. Lymph-node derived biopsies were excluded from this analysis. B: Peripheral immune phenotypes correlate with PFS-9 in NSCLC patients and PFS-6 in bladder cancer patients; I) Identification of plasmacytoid dendritic cells in the NSCLC cohort and correlation with PFS-9. PBMCs from pre-treatment, pre-vaccine and post-vaccine time points were analyzed using flow cytometry to quantify plasmacytoid DCs based on expression of CD123 and CD303. II) Identification of memory and naive $CD8^+$ T cells in the bladder cancer cohort and correlation with PFS-6. PBMCs from pre-treatment, pre-vaccine and post-vaccine time points were analyzed using flow cytometry to quantify memory $CD8^+$ T cell subsets based on expression of CD45RA and CD45RO. Data are presented as box and whisker plot with the box representing the 25th to 75th percentile, whiskers representing the min and max value and the horizontal line representingt the median. Statistical significance was determined using an unpaired t test. C: Presence of APOE4 genetic variant correlates with PFS-9 in melanoma, but not with PFS-9 in NSCLC or PFS-6 in bladder cancer; Patients with PFS-6/9 (green) and without PFS-6/9 (blue) in relation to presence or absence of an APOE4 germline genetic variant. Values are shown for the melanoma, NSCLC, and bladder cancer cohorts according to achieving 9-month month PFS for melanoma and NSCLC and 6 months PFS for bladder cancer, respectively. P values are calculated using Fisher's exact test. The numbers in each bar plot represents the number of patients.

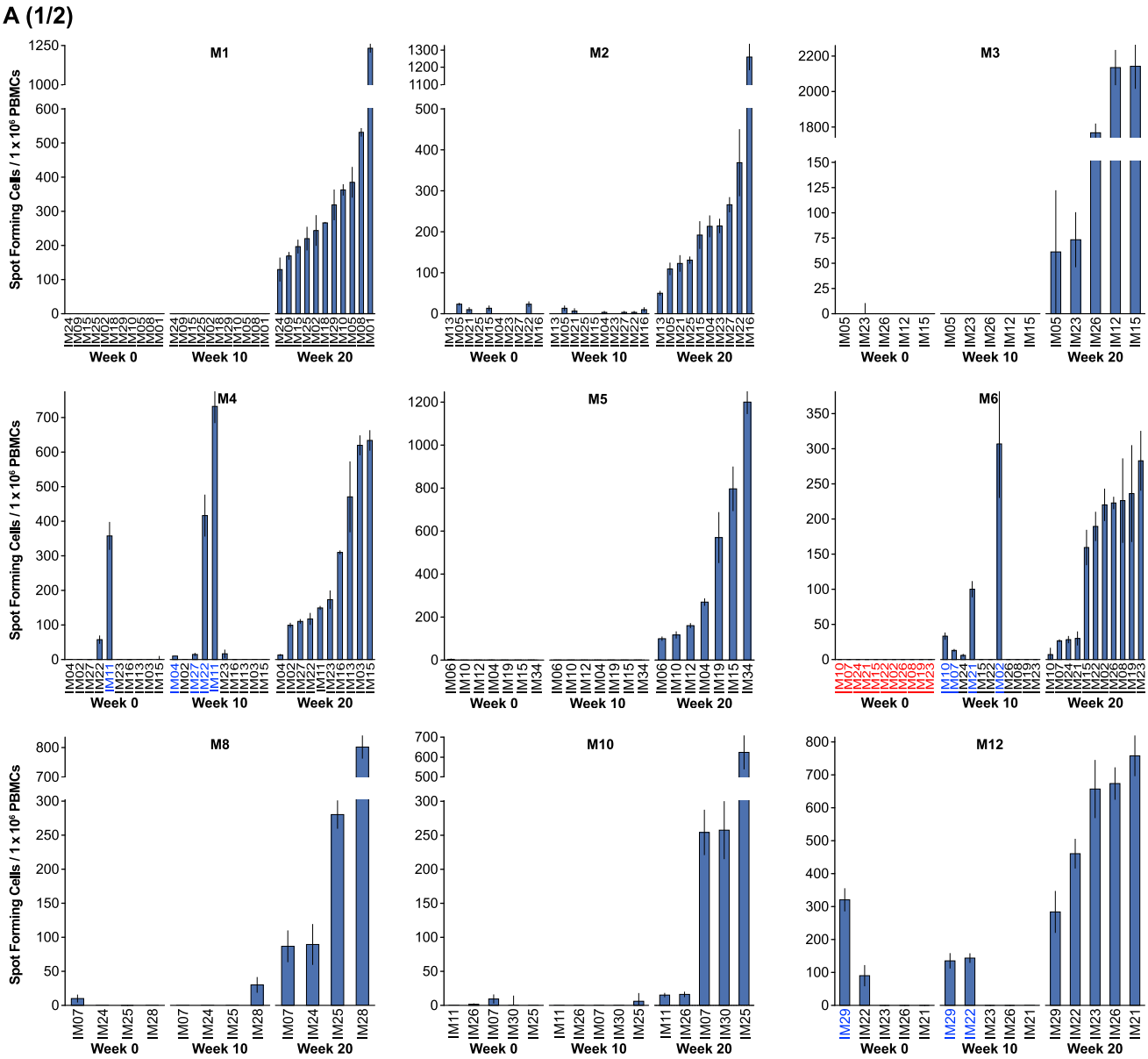

Figure S3. NEO-PV-01 Plus Anti-PD-1 Induces T Cell Reactivity against Multiple Vaccine Neoepitopes; Additional Data Related to Figure 4

A-C) T cell responses to individual immunizing (IM) peptides across 18 melanoma (A), 7 NSCLC (B) and 9 bladder (C) cancer patients are shown. Details of the assay are provided in the Method Details section. Immunizing peptides that did not elicit reactivity are not shown. Each IM peptide was tested for generation of an immune response using a series of overlapping peptides (Method Details) and the assay peptide generating the maximum response for each IM peptide are shown across the three time points. Each bar corresponds to an IM peptide and the assay peptide that generates the maximal response in either of the two assay formats (*ex vivo* assay or 5-day assay) for that IM peptide is shown. Immunizing peptides labeled in red on the x axis were not tested at the indicated time point due to limited sample availability whereas IM peptides labeled in blue on the x axis elicited pre-vaccine responses. Forty two percent of the neoantigen-specific responses detected were seen in an *ex vivo* assay and the remainder were detected in a 5-day assay with the neoantigen peptide in the absence of serum and cytokines. Vaccine response plots for patients M1, L1 and B1 are also depicted in the main Figure 4A. Aggregate data are represented as mean ± SEM.

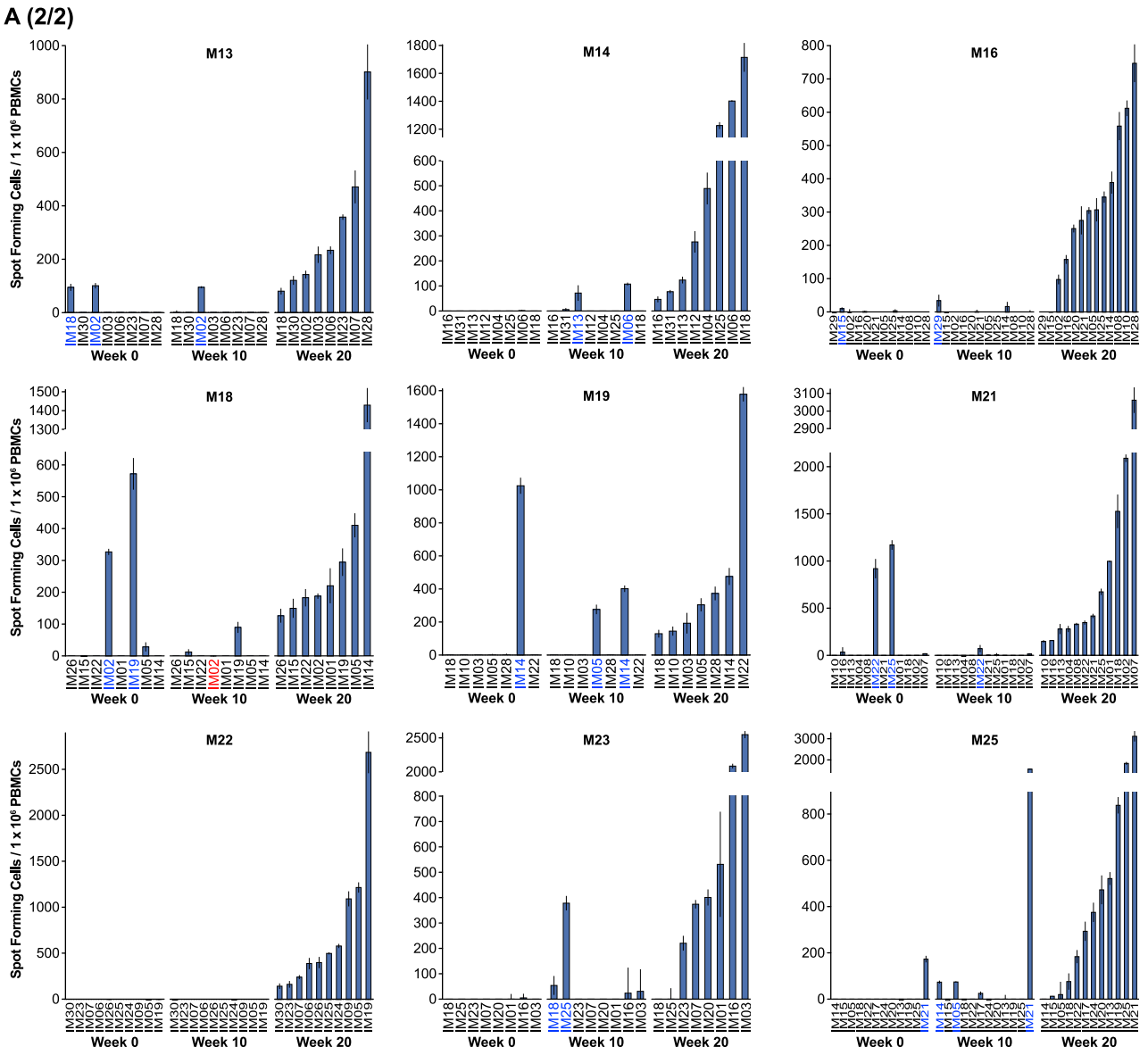

Figure S3. Continued

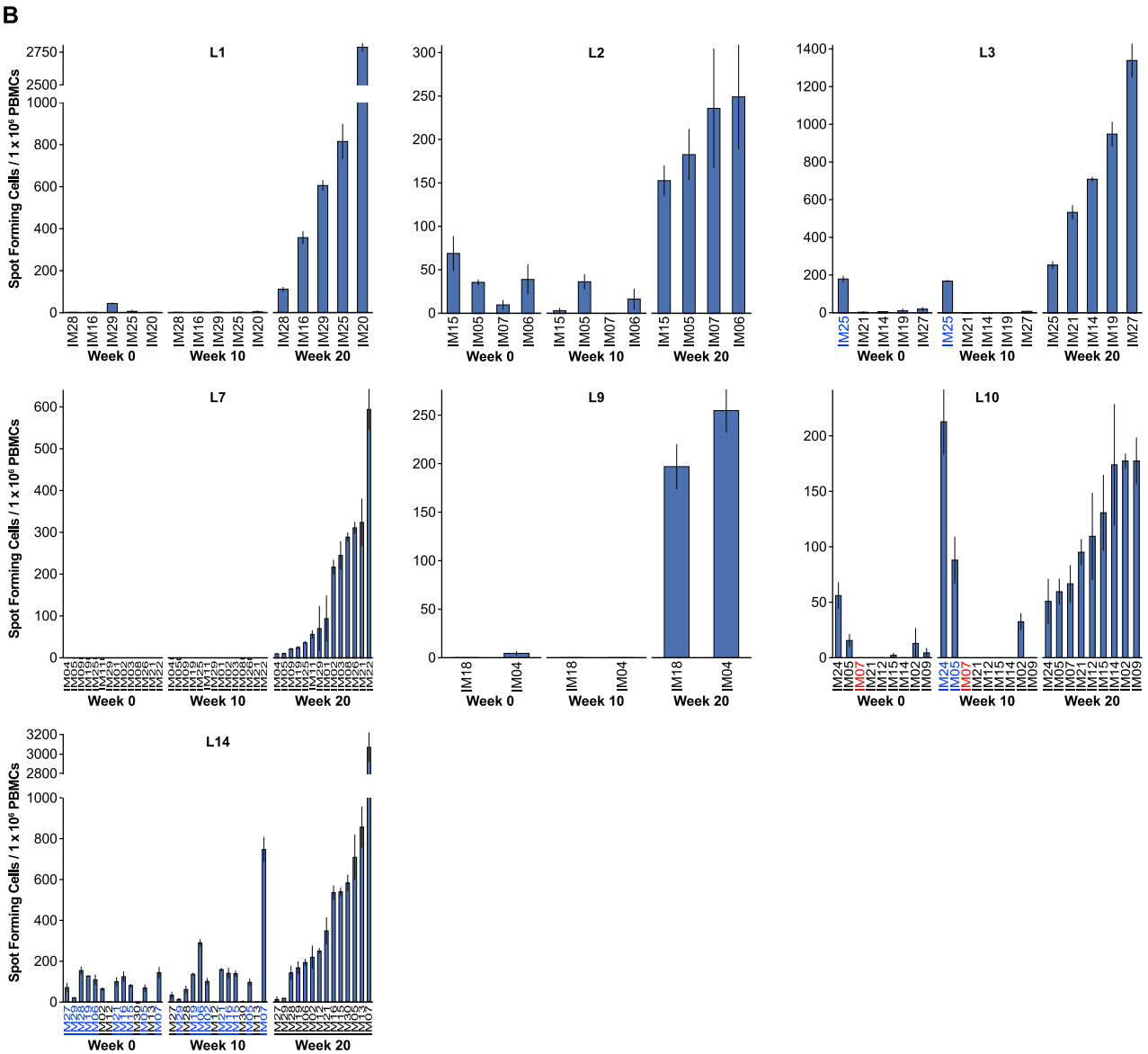

Figure S3. Continued

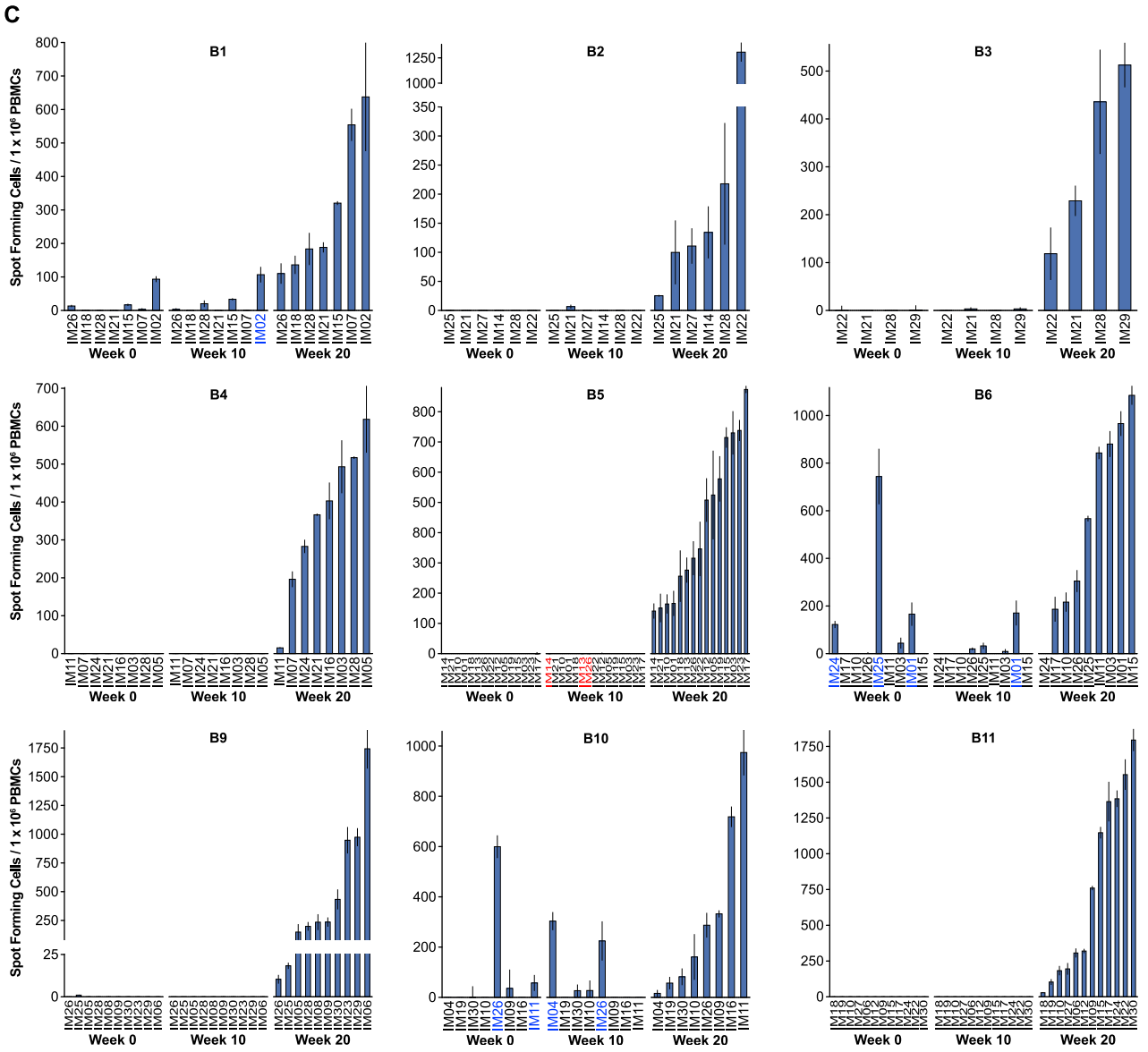

Figure S3. Continued

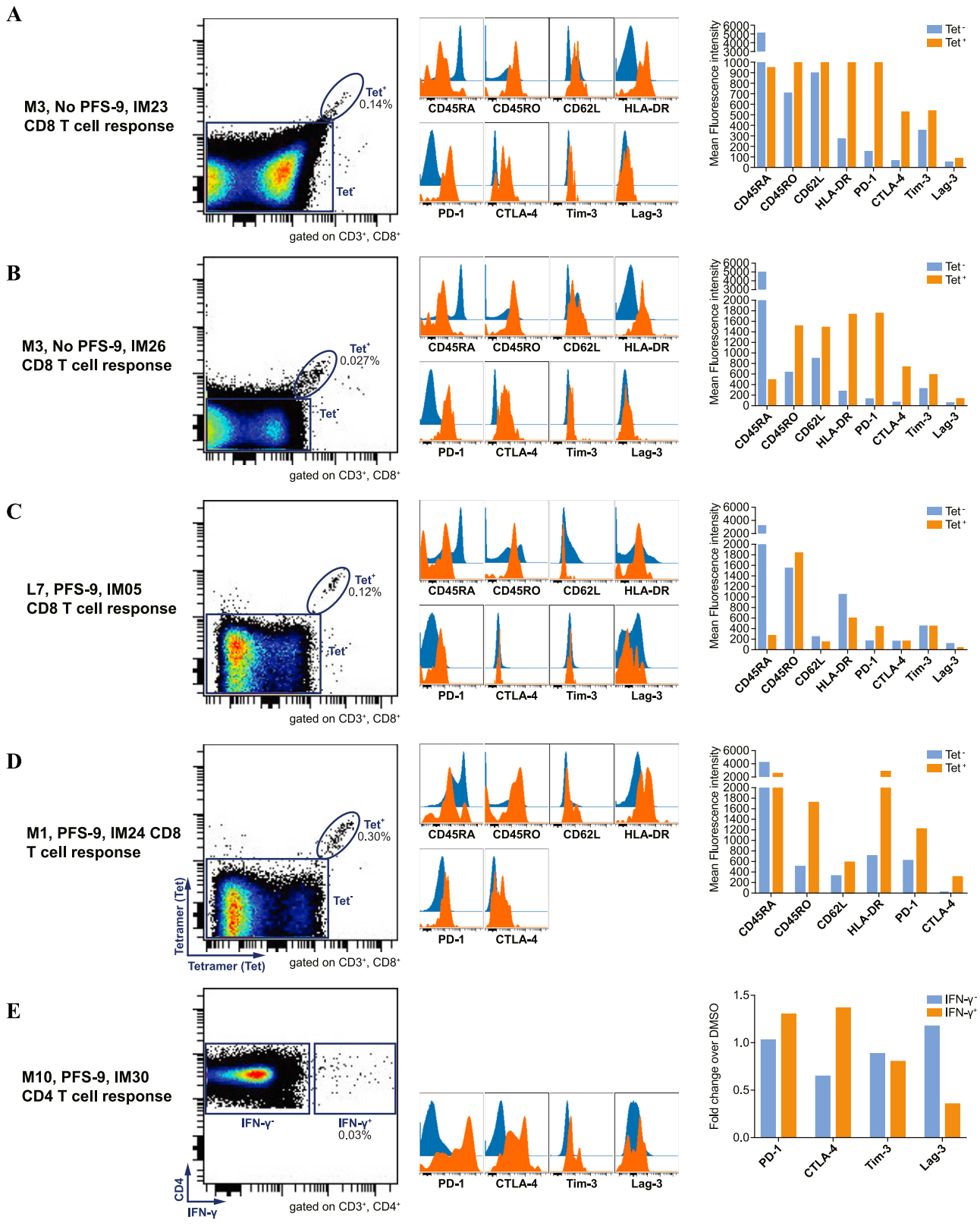

(legend on next page)

Figure S4. Phenotypic Analysis of CD4$^+$ and CD8$^+$ T Cells Induced by NEO-PV-01 Plus Anti-PD-1; Additional Data Related to Figure 4

Phenotypic analysis of neoantigen specific T cells by FACS for patients M3 (A) and (B), L7 (C), M1 (D) and M10 (E). Each row depicts phenotyping of an individual IM peptide. The left panel in each row depicts the FACS plot to identify the neoantigen specific T cell either by tetramer analysis (for CD8$^+$ T cell responses, A-D) or by a functional IFNγ assay (for CD4$^+$ T cell responses, E). The histogram plots in each row show the relative levels of the indicated marker between tetramer/ IFNγ positive T cells (orange) to the corresponding negative population (blue). Quantitation of the histogram plots are shown in the right panel. Tetramers used in this analysis are HLA- A11:01 (A), HLA-A68:01 (B), HLA-B81:01 (C) and HLA-B51:01 (D).

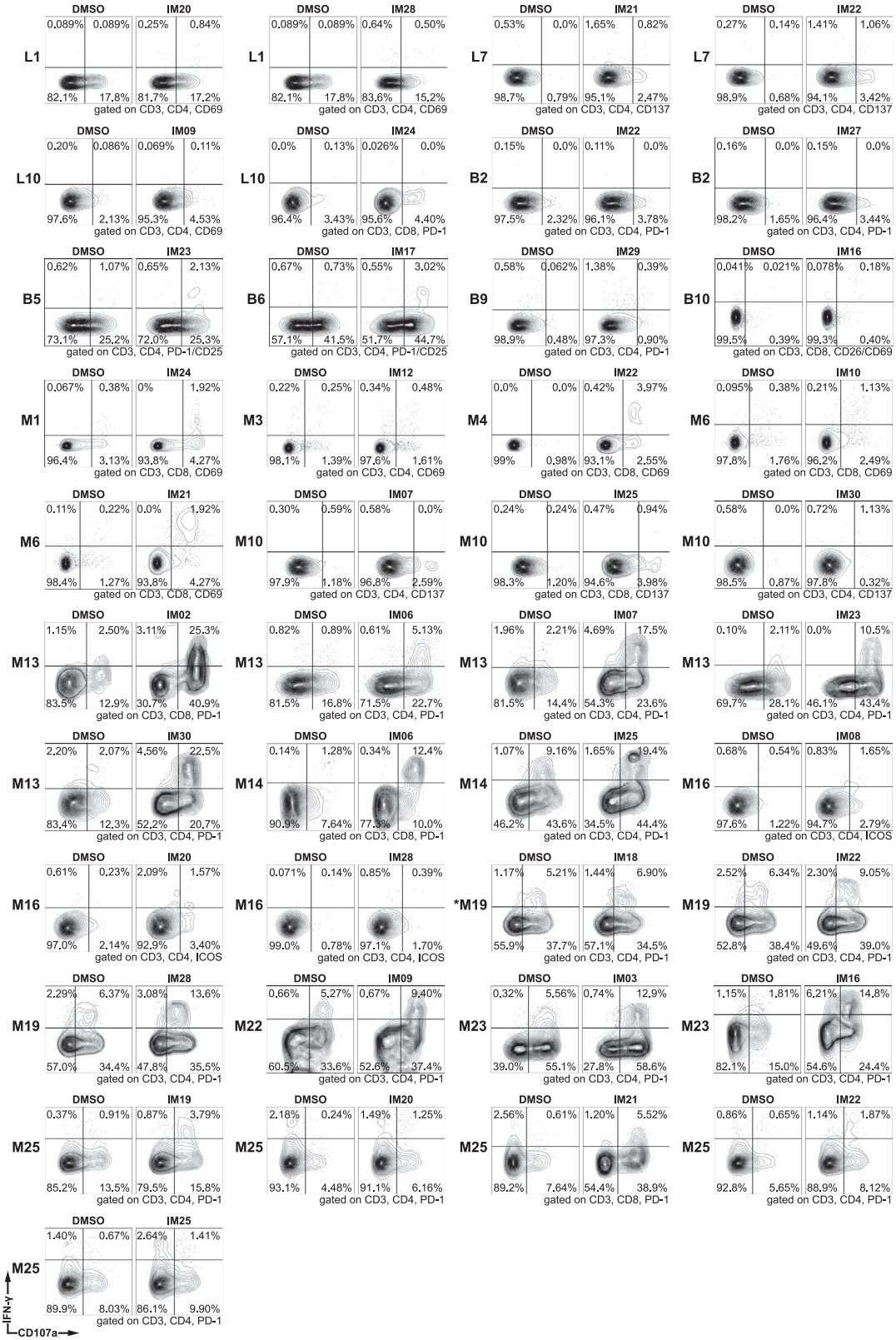

(legend on next page)

Figure S5. NEO-PV-01 Plus Anti-PD-1 Induces Cytotoxic CD4$^+$ and CD8$^+$ T Cell Responses; Additional Data Related to Figure 5

Surface expression of the cytolytic marker CD107a (x axis) and intracellular expression of IFNγ (y axis) is shown by FACS for 40 IM peptides across 19 patients. Individual plots depict control (DMSO) on the left and IM peptide on the right. Only IM peptides that were positive in this assay (> 1.5-fold stimulation over DMSO control in the CD107a positive or CD107a and IFNγ double positive gate are shown. Parent gates are indicated below each pair of FACS plots. *analysis done at the week 52 time point. Plot for patient M1 is also depicted in the main Figure 5B II.

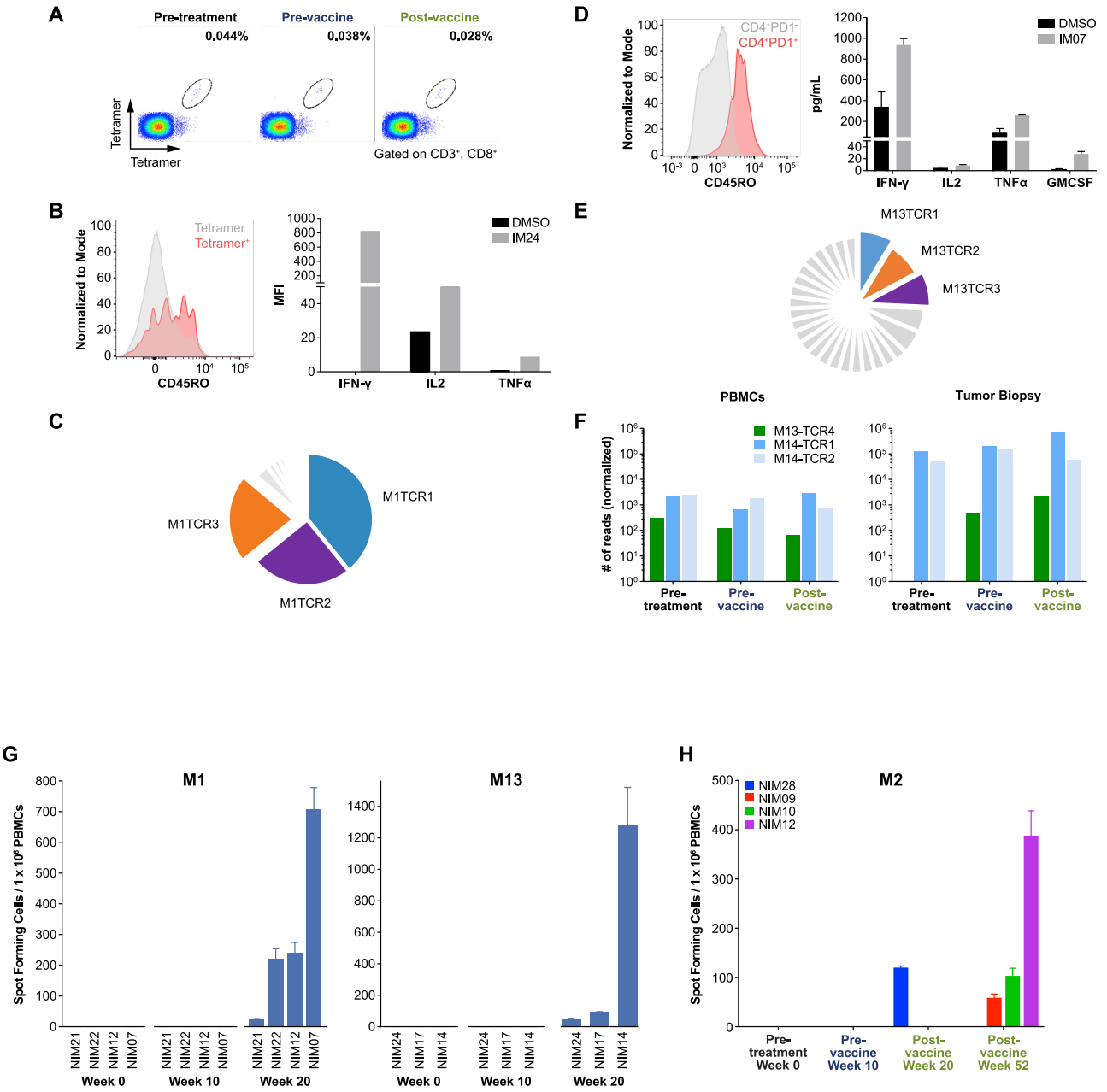

Figure S6. NEO-PV-01 Plus Anti-PD-1 Induces T Cells That Exhibit a Memory Phenotype, Are Polyfunctional, and Result in Epitope Spread; Additional Data Related to Figure 5

(A) Tetramer analysis of LMP2A-specific epitope in PBMCs of patient M1. B and C) Phenotype, function, and TCR clonotype of IM24-specific CD8$^+$ T cells from patient M1 at the post-vaccine time point. (B) Left panel: Overlaid histogram plot for CD45RO expression in IM24 tetramer positive and negative CD8$^+$ T cells. Right panel: Expression of cytokines as assessed by intracellular cytokine staining upon control (DMSO) and IM24 stimulation for 6 hours in IM24 tetramer positive CD8$^+$ T cells. (C) TCR clones identified by single cell TCR sequencing of IM24 tetramer-sorted T cells. D and E) Phenotype, function, and TCR clonotypes of IM07-specific CD4$^+$ T cells from patient M13 at the post-vaccine time point. (D) Left panel: Overlaid histogram plot for CD45RO expression in PD-1 positive and PD-1 negative T cells upon stimulation with IM07. Right panel: Cytokine secretion after 40h as assessed by ELISA. (E) TCR clones identified by single cell TCR sequencing of IM07-specific sorted T cells. (F) Identities of three additional validated neoantigen-specific TCRs from two melanoma patients (M13 and M14) and their frequencies in PBMC and tumor biopsy. (G) Epitope spread in melanoma patients M1 (left panel) and M13 (right panel). Reactivity of post-vaccine PBMCs against predicted neoantigen peptides that were not included in the vaccine were tested by IFNγ ELISpot assay at the three indicated time points. (H) Epitope spread in melanoma patient M2 who had a CR, across 4 time points. Only peptides that elicited responses are shown. NIM: Non-immunizing neoepitope. Aggregate data are represented as mean ± SEM.